

AUTO PQ: AUTOMATING QUANTILE ESTIMATION FROM POINT FORECASTS IN THE CONTEXT OF SUSTAINABILITY

 **Stefan Meisenbacher**

Institute for Automation and Applied Informatics
Karlsruhe Institute of Technology
Eggenstein-Leopoldshafen, 76344, Germany
stefan.meisenbacher@kit.edu

 **Kaleb Phipps**

Scientific Computing Center (SCC)
Karlsruhe Institute of Technology
Eggenstein-Leopoldshafen, 76344, Germany

 **Oskar Taubert**

Scientific Computing Center (SCC)
Karlsruhe Institute of Technology
Eggenstein-Leopoldshafen, 76344, Germany

 **Marie Weiel**

Scientific Computing Center (SCC)
Karlsruhe Institute of Technology
Eggenstein-Leopoldshafen, 76344, Germany

 **Markus Götz**

Scientific Computing Center (SCC)
Karlsruhe Institute of Technology
Eggenstein-Leopoldshafen, 76344, Germany

 **Ralf Mikut**

Institute for Automation and Applied Informatics
Karlsruhe Institute of Technology
Eggenstein-Leopoldshafen, 76344, Germany

 **Veit Hagenmeyer**

Institute for Automation and Applied Informatics
Karlsruhe Institute of Technology
Eggenstein-Leopoldshafen, 76344, Germany

ABSTRACT

Optimizing smart grid operations relies on critical decision-making informed by uncertainty quantification, making probabilistic forecasting a vital tool. Designing such forecasting models involves three key challenges: accurate and unbiased uncertainty quantification, workload reduction for data scientists during the design process, and limitation of the environmental impact of model training. In order to address these challenges, we introduce AutoPQ, a novel method designed to automate and optimize probabilistic forecasting for smart grid applications. AutoPQ enhances forecast uncertainty quantification by generating quantile forecasts from an existing point forecast by using a conditional Invertible Neural Network (cINN). AutoPQ also automates the selection of the underlying point forecasting method and the optimization of hyperparameters, ensuring that the best model and configuration is chosen for each application. For flexible adaptation to various performance needs and available computing power, AutoPQ comes with a default and an advanced configuration, making it suitable for a wide range of smart grid applications. Additionally, AutoPQ provides transparency regarding the electricity consumption required for performance improvements. We show that AutoPQ outperforms state-of-the-art probabilistic forecasting methods while effectively limiting computational effort and hence environmental impact. Additionally and in the context of sustainability, we quantify the electricity consumption required for performance improvements.

Keywords Probabilistic time series forecasting · Uncertainty quantification · AutoML · Energy Consumption

1 Introduction

Uncertainty quantification is necessary for making informed decisions in smart grid applications, rendering probabilistic time series forecasts essential [1]. Exemplary downstream applications are stochastic power flow optimizations [2, 3], smart charging of stationary battery systems and electric vehicles [4–7], and economic dispatch [8, 9]. As the number of applications increases, automating the design process of probabilistic time series forecasting models is necessary to keep pace with the growing demand.

This process involves three major challenges: First, a forecast’s inherent uncertainty must be quantified in an unbiased and accurate manner. However, many recently published methods [10–12] only provide point forecasts [13]. Methods to generate a probabilistic forecast from a point forecast exist but have limitations, e. g. they assume a Probability Density Function (PDF) [14, 15], only estimate Prediction Intervals (PIs) [16, 17], or rely on the residuals of the point forecast [18] instead of representing the uncertainty of the process itself. Although direct probabilistic methods can partially overcome these limitations, they fail to leverage the many existing and well-established forecasting models already in use [19].

Second, given that the forecast quality is sensitive to different model design decisions [20], no forecasting method can excel in all tasks (no-free-lunch theorem), and the quality requirements depend on the downstream application. That is why automatically selecting the best-performing method is absolutely crucial [19]. In addition, performance-critical smart grid applications often demand further model enhancement by Hyperparameter Optimization (HPO). However, existing Combined Algorithm Selection and Hyperparameter optimization (CASH) methods in time series forecasting are limited to point forecasting [21–23] or are subject to the constraints outlined in the first challenge [24].

Third, methodological advances in probabilistic forecasting must quantify the environmental impact of employing such an advanced model in a standardized, quantifiable, and comparable manner [25]. Specifically, smart grid applications utilizing forecasts must ensure that the electricity consumption required for forecasting model design remains at a reasonable level. This is crucial because excessive electricity consumption, particularly for computationally intensive modern Deep Learning (DL) methods, can undermine sustainability efforts by increasing the overall carbon footprint. Despite this need, most existing probabilistic forecasting methods only specify the computing hardware employed [24, 26, 27] but fail to report the associated electricity consumption.

To tackle these challenges, we introduce AutoPQ, a novel method for automated and electricity consumption-aware quantile forecasts from point forecasts. Our key contributions include:

- AutoPQ generates quantile forecasts without requiring prior information about the underlying distribution by i) using established point forecasting methods (unknown distribution), ii) mapping the point forecast into the latent space of a conditional Invertible Neural Network (cINN) [28] (known and tractable distribution), and iii) sampling in the neighborhood of the point forecast’s latent space representation [19].
- AutoPQ enhances [19] and automates model design decisions by *a*) optimizing the variance for sampling in the latent space, *b*) selecting the best-performing point forecasting method, and *c*) optimizing its hyperparameters.
- In order to accommodate various computing systems and performance requirements, we introduce AutoPQ-`default` (automating *a* and *b*) for general-purpose computing systems to provide high-quality probabilistic forecasts, and AutoPQ-`advanced` (automating *a*, *b*, and *c*) for High-Performance Computing (HPC) systems to increase the forecasting quality further, as required by smart grid applications with high decision costs. Additionally, the electricity consumption of AutoPQ-`default` and AutoPQ-`advanced` is reported and compared in relation to their achievable performance.

The remainder of the paper is structured as follows: Section 2 provides an overview of relevant related work. In Section 3 we then present AutoPQ, which we further evaluate in Section 4. The results of our evaluation are discussed in Section 5. Finally, Section 6 gives a conclusion and an outlook.

2 Related work

This section analyzes related work with a particular focus on the three challenges stated above, i. e., uncertainty quantification in time series forecasting, design process automation, and quantification of energy consumption required for performance improvements. Table 1 gives an overview of the analyzed literature.

2.1 Probabilistic time series forecasting

Probabilistic time series forecasting methods can be categorized into direct probabilistic methods and probabilistic methods based on point forecasts.

Direct probabilistic forecasting methods. Direct probabilistic forecasting methods aim to learn the uncertainty of the forecast during model training. Depending on how a forecast’s uncertainty is represented, they can be divided into quantile-based, distribution-based, and normalizing flow-based forecasts.

Quantile-based forecasting methods are trained to represent certain quantiles. These quantiles can then be applied

Table 1: Overview of existing time series forecasting methods in terms of uncertainty quantification, automated design, and reporting the electricity consumption for the model design.

Reference	Category	Uncertainty quantification			Automated design	Electricity consumption
		Quantiles/Pis	PDF	Scenarios		
[29, 30]	Direct probabilistic forecast	✓	✗	✗	✗	✗
[26]	Direct probabilistic forecast	✓	✓	✗	✗	✗
[27]	Direct probabilistic forecast	✓	✓	✗	HPO	✗
[31–39]	Direct probabilistic forecast	✓	✓	✓	✗	✗
[14, 16, 17, 40, 41]	Point forecast-based probabilistic forecast	✓	✗	✗	✗	✗
[18]	Point forecast-based probabilistic forecast	✓	✓	✓	✗	✗
[15]	Point forecast-based probabilistic forecast	✓	✓	✗	✗	✗
[42–51]	Point forecast	✗	✗	✗	HPO	✗
[21–23]	Point forecast	✗	✗	✗	CASH	✗
[24]	Point forecast-based and direct probabilistic forecast	✓	✗	✗	CASH	✗
AutoPQ-default	Point forecast-based probabilistic forecast	✓	✓	✓	HPO	✓
AutoPQ-advanced	Point forecast-based probabilistic forecast	✓	✓	✓	CASH	✓

Hyperparameter Optimization (HPO), Combined Algorithm Selection and Hyperparameter optimization (CASH)

to derive PIs with a specific conditional probability that the target value lies within the interval. For instance, a Quantile Regression Neural Network (QRNN) [29] uses the Pinball Loss (PL) function during training such that the resulting forecast represents a specific quantile. Multiple QRNNs representing different quantiles can be trained to forecast this set of quantiles. A different approach is the Nearest Neighbor Quantile Filter (NNQF) [30] that modifies the training dataset based on similarity in the target variable to determine a set of quantiles. Afterward, the method trains a Machine Learning (ML)-based method on the modified data to forecast this set of quantiles.

However, both QRNNs and the NNQF can only forecast quantiles, from which PIs can be derived, but do not provide the probability distribution.

The full PDF or Cumulative Distribution Function (CDF) can be obtained from distribution-based forecasts. A well-known example is Deep AutoRegression (DeepAR) [26], an AutoRegression (AR)-based Recurrent Neural Network (RNN) trained to learn the parameters of a given PDF and generate probabilistic forecasts by sampling from it. In [27], the authors extend DeepAR to make probabilistic hierarchical forecasts. However, both methods require assuming the underlying PDF, which is limiting if the data does not follow a standard parametric distribution.

This disadvantage is overcome by normalizing flow-based probabilistic forecasts, which learn a bijective mapping from the unknown PDF of the data to a known and tractable PDF. Typically, normalizing flows are used to enhance existing probabilistic forecasting methods, such as QRNNs [31], RNNs [32], Gaussian mixture models [33], and Bernstein polynomials [34]. They can also be applied to directly generate probabilistic forecasts for various domains, including atmospheric variables [35], renewable energy generation [38], electrical load [36–38], and electricity prices [39]. Although these methods are effective, many do not consider exogenous features like weather variables to condition the PDF, i. e., they assume that the learned distribution remains constant.

All direct probabilistic forecasting methods are limited by their inability to generate probabilistic forecasts from available, well-designed point forecasts [13].

Point forecast-based probabilistic forecasting methods.

Point forecast-based probabilistic forecasting methods quantify forecast uncertainty using a separate approach for uncertainty estimation [52]. In this context, most uncertainty quantification methods rely on the residuals between point forecasts and observed values in a validation dataset to estimate PIs. The assumptions regarding the distribution of the residuals differ between methods. For instance, they can be assumed to follow a Gaussian distribution [14], an empirical distribution [16], or an empirical non-conformity score distribution [17, 40, 41]. The latter calculates a critical non-conformity score for the desired significance level of the PI by assessing how unusual a residual is compared to other residuals in the validation dataset. However, these methods can only estimate PIs and do not provide the full PDF.

Beyond the above approaches, there are enhancements in residual-based uncertainty quantification that leverage ML techniques. In [18], the authors train a Generative Adversarial Network (GAN) on the residuals of a point forecast, which is subsequently used to generate residual scenarios and quantify the point forecast’s uncertainty. In [15], a Gaussian distribution of residuals is assumed, and an Artificial Neural Network (ANN) is trained to forecast the standard deviation of these residuals. The estimated standard deviation is then used to quantify the point forecast’s uncertainty. As the uncertainty estimation models are trained on the point forecast’s residuals, both approaches directly depend on the point forecast. Consequently, when comparing multiple candidate point forecasting methods and hyperparameter configurations, a separate uncertainty estimation model must be trained for each of them.

2.2 Automated time series forecasting

Automated time series forecasting methods can be classified into two main categories: Hyperparameter Optimiza-

tion (HPO) and Combined Algorithm Selection and Hyperparameter optimization (CASH). While automated point forecasting utilizing HPO [42–51] and CASH [21–23] has been extensively researched, there is a significant gap in studies that focus on automated probabilistic forecasting [53].

Hyperparameter optimization. The purpose of HPO is to find a forecasting method’s configuration that delivers the best-possible performance for a given forecasting task.

Simple grid search-based HPO has been proposed for point forecasting methods within the Statistical Modeling (SM) family, such as Error Trend Seasonality (ETS) [42], seasonal AutoRegressive Integrated Moving Average with eXternal input (sARIMAX) [43], and Trigonometric seasonality, Box-Cox transformation, ARMA errors, Trend, Seasonal components (TBATS) [44]. Grid search is also utilized within the ML family, e. g., for HPO of point forecasting methods based on Support Vector Regression (SVR) [45, 46]. While effective for small configuration spaces, higher-dimensional spaces require HPO algorithms that explore the configuration space more efficiently. For example, random search is more efficient than grid search [54] and is widely applied for HPO of ML-based point forecasting methods such as the Gradient Boosting Machine (GBM) [48] and the MultiLayer Perceptron (MLP) [47]. For a directed search of complex configuration spaces, such as for methods of the DL family, gradient-based search methods [49], Bayesian Optimization (BO) [50], and Evolutionary Algorithms (EAs) [51] are used. Aside from point forecasting methods, these HPO techniques can also be applied to DL-based direct probabilistic forecasting methods, as demonstrated in [27]. Although HPO of a single forecasting method is effective, it neglects the no-free lunch theorem, stating that no single forecasting method excels at all forecasting tasks.

Combined algorithm selection and hyperparameter optimization. To select the best-performing forecasting method with optimized hyperparameters, several CASH methods are available for point forecasting. In [21], the authors take different ML-based forecasting methods into account, including Least Absolute Shrinkage and Selection Operator (LASSO), Random Forest (RF), eXtreme Gradient Boosting (XGB), MLP, and SVR, and use BO for solving the CASH problem. Similar approaches exist in [22] and [23], additionally considering point forecasting methods of the SM family (e. g., AutoRegressive Integrated Moving Average (ARIMA), Triple Exponential Smoothing (TES), and Box-Cox transformation, ARMA errors, Trend, Seasonal components (BATS)) and the DL family (e. g., Neural Hierarchical Interpolation for Time Series (N-HiTS) and Temporal Fusion Transformer (TFT)). Apart from the application to point forecasting, CASH methods are also used for direct and point forecast-based probabilistic forecasting [24]. In their CASH problem, the authors consider several direct probabilistic forecasting methods, like DeepAR, as well as point forecasting methods of the

SM and ML family using conformal PIs to derive probabilistic forecasts. Despite their contribution to addressing the under-researched area of CASH for probabilistic forecasting, the applied uncertainty quantification methods are still subject to the aforementioned limitations, i. e., require assuming the underlying PDF and do not take into account the conditioning of the PDF by exogenous features.

2.3 Computing effort for methodological advances

Regarding the quantification of efforts required for performance improvements, the above-reviewed related works exhibit significant shortcomings. While some of the studies specify the used hardware and required training duration [21, 23, 24, 26, 30, 35, 38, 45, 49], estimating the corresponding energy consumption from this information involves considerable effort, with inherent uncertainty. Yet, the electricity consumption is an essential metric as it is independent of data center-specific or geopolitical factors at the time of measurement [25]. Once electricity consumption is quantified, other metrics, such as the carbon footprint or the monetary costs, can be derived using assumed or local conditions.

3 AutoPQ

To address the three key challenges in the automated design of probabilistic time series forecasting models, we present AutoPQ, an innovative method for electricity consumption-aware quantile forecasting based on point forecasts. The idea behind AutoPQ is to use a cINN [28] to generate a probabilistic forecast from any arbitrary point forecast [19] while automatically making corresponding design decisions to enhance probabilistic performance. In the following section, we describe i) the generation of such a probabilistic forecast, ii) the corresponding design decisions, and iii) the automation of these decisions, highlighted green in Figure 1. To accommodate various computing systems and performance requirements, we propose two variants of AutoPQ: AutoPQ-`default`, designed for general-purpose computing systems and capable of providing high-quality probabilistic forecasts [19], and AutoPQ-`advanced`, which requires HPC systems¹ to further increase forecasting quality for downstream applications with high decision costs.

3.1 Creation of the probabilistic forecast

Generating a probabilistic forecast with a cINN using a point forecast involves three steps [19].²

Creation of a point forecast in an unknown distribution. A point forecast is generated using an arbitrary point forecasting model $f_p(\cdot)$, which estimates

¹In this paper, we refer to servers for parallel computing with multiple nodes and Graphics Processing Unit (GPU) acceleration as HPC systems.

²For a detailed description, we refer to [19].

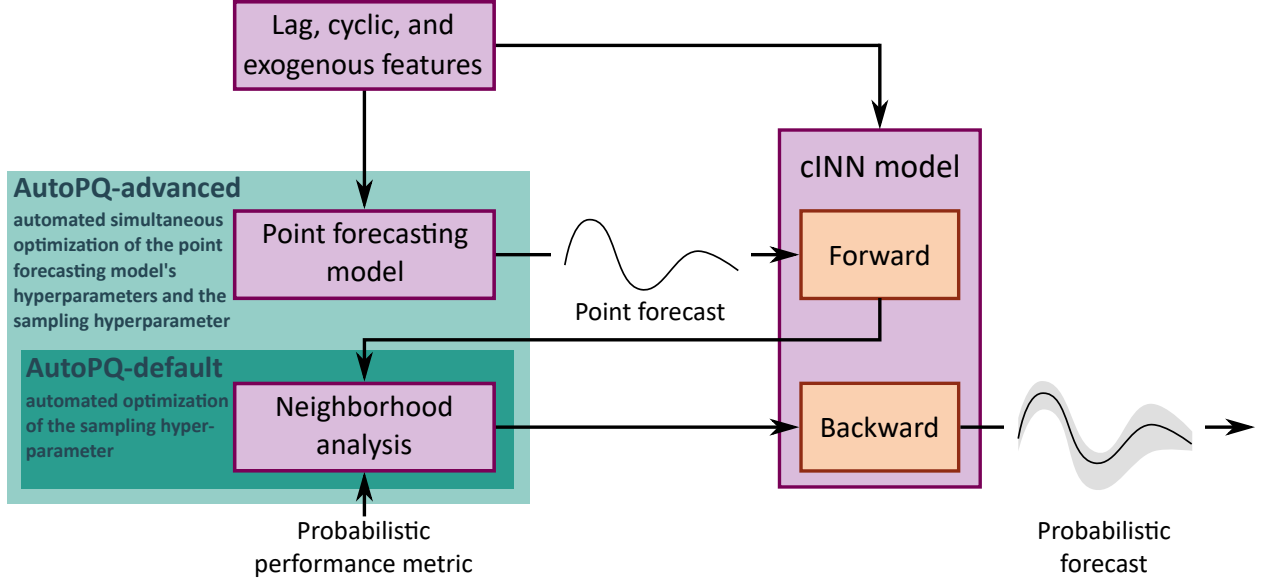


Figure 1: Overview of AutoPQ: Lag features, seasonal features, and exogenous features are selected and used as inputs by a point forecasting model to generate a point forecast in an unknown distribution. This point forecast and the features are combined in a cINN, resulting in a representation of the forecast in a known and tractable distribution. The neighborhood of this representation is analyzed to determine how to include uncertainty information. Finally, with the backward pass through the cINN, the uncertainty is mapped back to the unknown distribution to generate the probabilistic forecast. Automation methods are highlighted in green.

future values \hat{y} of the target time series \mathbf{y} using current and past values. More precisely, the model $f_p(\cdot)$ makes a forecast $\hat{y}[k+1, \dots, k+H]$ for a specified forecast horizon $H \in \mathbb{N}_1$ at origin k , taking into account historical values of $\mathbf{y}[k-H_1, \dots, k]$, values of exogenous forecasts $\hat{\mathbf{X}}[k+1, \dots, k+H]$, and exogenous time series $\mathbf{X}[k-H_1, \dots, k]$. Since the target time series \mathbf{y} contains realizations of \hat{y} , a point forecast can be interpreted as a sample of the random variable $Y \sim f_Y(\mathbf{y})$ in the realization space \mathbb{Y} with an unknown H -dimensional PDF $f_Y(\mathbf{y})$.

Representation of the point forecast in a known and tractable distribution. The point forecast $\hat{y}[k+1, \dots, k+H]$ as a sample from the unknown distribution is represented in a space with a known and tractable H -dimensional PDF $f_Z(\mathbf{y})$ using a cINN. The cINN learns a conditional³ and bijective function $g: \mathbb{Y} \rightarrow \mathbb{Z}$ [55] from the realization space \mathbb{Y} with unknown distribution into the latent space \mathbb{Z} with a multi-dimensional Gaussian distribution. This bijective function can be used to quantify the point forecast’s uncertainty by mapping it into the latent space and analyzing its neighborhood as described in the following. Notably, the training of the cINN is independent of the point forecasting model, which allows using one cINN to generate probabilistic forecasts from multiple arbitrary point forecasts.

³The cINN can include additional exogenous information into the mapping using conditional-affine coupling blocks [55].

Neighborhood analysis of the point forecast’s latent space representation. To obtain the point forecast’s latent space representation, the point forecast $\hat{y}[k+1, \dots, k+H]$ itself and additional exogenous information $\{\mathbf{y}[k-H_1, \dots, k], \mathbf{X}[k-H_1, \dots, k], \hat{\mathbf{X}}[k+1, \dots, k+H]\}$ are passed forward through the trained cINN. To quantify the point forecast’s uncertainty, the neighborhood of this representation is analyzed. Samples are generated in the Gaussian-distributed latent space with a sampling variance σ , resulting in a set of realizations that are similar but not identical to the original point forecast. These samples represent the uncertainty in the neighborhood of the point forecast’s latent space representation and can be passed backward through the cINN to calculate the quantiles of the probabilistic forecast $\hat{y}^*[k+1, \dots, k+H]$.⁴

3.2 Task-dependent design decisions

Generating a quantile forecast requires specific design decisions tailored to the forecasting task. These include feature engineering, selecting the point forecasting method and its hyperparameters λ_p , and choosing the sampling variance $\lambda_q = \sigma$ for generating a quantile forecast with the cINN based on the point forecast’s latent space representation.

Lag, cyclic, and exogenous features. Additional explanatory variables can enrich the input space of both the

⁴This is valid due to the equivalence of uncertainty in both spaces [19].

point forecasting model and the cINN. Lag features provide past values for the model as historical context. In the evaluation, point forecasting methods based on ML regression estimators require the explicit definition of lag features

$$x_{\text{lag}, H_1} [k] = x [k - H_1], \quad (1)$$

unlike SM- and DL-based forecasting methods that consider past values implicitly. Seasonal features represent cyclic relationships, such as the hour of the day or the month,

$$x_{s12} [k] = \sin \left(\frac{2\pi \cdot \text{month} [k]}{12} \right), \quad x_{c12} [k] = \cos \left(\frac{2\pi \cdot \text{month} [k]}{12} \right), \quad (2)$$

$$x_{s24} [k] = \sin \left(\frac{2\pi \cdot \text{hour} [k]}{24} \right), \quad x_{c24} [k] = \cos \left(\frac{2\pi \cdot \text{hour} [k]}{24} \right), \quad (3)$$

as well as work and non-work days:

$$x_{\text{wd}} [k] = \begin{cases} 1, & \text{if } \text{work_day}(k) \text{ is True,} \\ 0 & \text{otherwise.} \end{cases} \quad (4)$$

Since energy time series for smart grid applications contain predominantly daily, weekly, and yearly patterns [56–58], we consider seasonal features in the evaluation. Exogenous features are important if the target variable is influenced by external factors, such as weather conditions including temperature, humidity, wind speed, and solar irradiance. We thus select exogenous features depending on existing additional variables of the datasets in our evaluation [19].

Point forecasting methods and hyperparameters. As the point forecasting method in the above-described cINN approach significantly affects the probabilistic forecasting performance [19], we consider established methods from different forecasting method families in order to obtain a representative selection of methods that have proven effective and differ in their approach or architecture.

Statistical Modeling (SM): sARIMAX, ETS, TBATS,

Machine Learning (ML): MLP, SVR, XGB,

Deep Learning (DL): DeepAR, N-HiTS, TFT.

Since HPO can enhance performance beyond a method’s default configuration, we apply HPO on the configuration spaces detailed in Table A4, A5, and A6 in the Appendix.

Sampling hyperparameter of the latent space. The hyperparameter $\lambda_q = \sigma$ for generating samples from the point forecast’s latent space representation controls the magnitude of quantified uncertainty in the forecast: A larger σ includes more uncertainty and improves coverage rates, while a smaller σ produces sharper probabilistic forecasts. Both coverage rate and sharpness can be evaluated using probabilistic performance metrics, enabling HPO to tailor the sampling hyperparameter $\lambda_q = \sigma$ to the forecasting task [59]. The considered value range is given in Table A1 in the Appendix.

3.3 Optimal design of the probabilistic forecast

AutoPQ automates the design decisions outlined above by optimally configuring the forecasting model. We propose AutoPQ-default for general-purpose computing systems to provide high-quality probabilistic forecasts, and AutoPQ-advanced for HPC systems to enhance the performance further.

3.4 AutoPQ-default for general-purpose computing systems

Given the high computational effort of HPO for point forecasting methods illustrated in Figure 2, AutoPQ-default only focuses on optimizing the sampling hyperparameter to provide high-quality point forecast-based quantile forecasts using general-purpose computing systems for the model design.

Hyperparameter optimization. Instead of manually exploring a given configuration space Λ_q to find the (estimated) optimal hyperparameter configuration λ_q^* , we define the HPO problem

$$\lambda_q^* = \min_{\lambda \in \Lambda_q} Q(\hat{\mathbf{y}}(\lambda_q), \mathbf{y}), \quad (5)$$

with an arbitrary probabilistic performance metric as objective function Q and the hyperparameter λ_q for generating samples from the point forecast’s latent space representation.

Optimization algorithm. Given that the objective function Q (5) is potentially noisy and non-differentiable and we do not have a closed-form expression of the configuration space Λ_q , we use the black-box optimizer Hyperopt [60]. Hyperopt acts as the HPO trial generator suggesting new candidate configurations to be assessed. The suggestion is based on BO using the Tree Parzen Estimator (TPE) as surrogate model, which balances exploration and exploitation of promising regions in the configuration space.

Early stopping. The optimization can be stopped once the objective function’s value Q has converged or reached a satisfactory value. To terminate the BO when additional trials are unlikely to improve Q , we use early stopping upon Q reaching a plateau, defined as the standard deviation of the five best trials falling below 0.0005, with a patience of five trials.⁵

Forecasting method selection. Probabilistic forecasting performance depends on not only the hyperparameter λ_q but also the underlying point forecasting method. In order to address this, AutoPQ-default selects the best-performing point forecasting method while optimizing the corresponding λ_q . First, all candidate point forecasting

⁵Note that the assessment is performed on normalized data, i. e., the values of Q across datasets are in similar ranges.

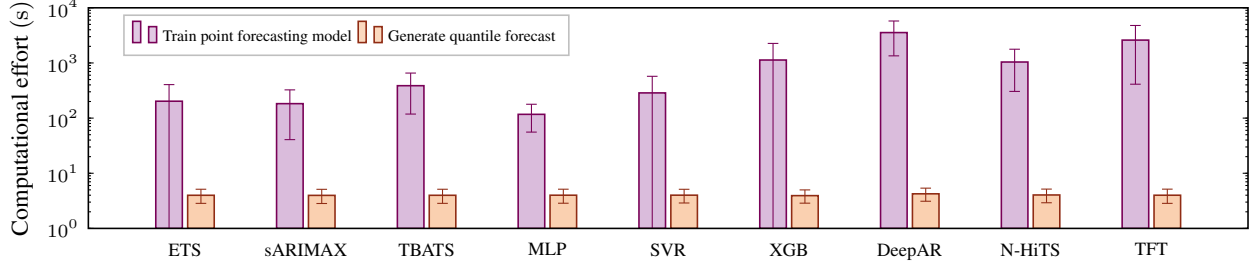


Figure 2: Comparison of the average computational effort in terms of runtime across the six datasets used in the evaluation: effort for training a point forecasting model with configuration λ_p and effort for generating a quantile forecast based on the point forecast using the cINN with λ_q . Due to the significantly smaller computational effort of generating the quantile forecast, it is worthwhile to evaluate several λ_q for one λ_p to properly balance the efforts. Note that for ETS, SVR, and XGB the standard deviation is higher than the mean value.

models are trained with default configurations $\lambda_{p,\text{default}}$. A quantile forecast is then generated for each model, with the associated sampling hyperparameter λ_q optimized with the previously described HPO. Finally, the combination of point forecasting model and optimized sampling hyperparameter achieving the best score on the validation dataset is selected.

3.4.1 AutoPQ-advanced for HPC systems

In smart grid applications with high decision costs, improving probabilistic forecasting performance is vital. AutoPQ-advanced addresses this requirement using HPC systems for the model design as detailed in the following.

Hyperparameter optimization. Similarly to AutoPQ-default (5), the HPO problem

$$\lambda^{\star} = \min_{\lambda \in \Lambda} Q(\hat{y}(\lambda_p, \lambda_q), y) \quad (6)$$

is defined, with an arbitrary probabilistic performance metric as the objective function Q . In contrast to AutoPQ-default, AutoPQ-advanced considers the point forecasting method’s hyperparameter configuration λ_p together with the sampling hyperparameter λ_q for generating samples from the point forecast’s latent space representation.

In order to solve (6) efficiently, the computing times between training the point forecasting model and generating a quantile forecast based on this point forecast must be properly balanced. Figure 2 compares these efforts across the six evaluation datasets. Since generating a quantile forecast can be repeatedly refined with different sampling hyperparameters, we use two nested loops to solve (6) as outlined in Algorithm 1. The following paragraphs detail this joint optimization, the application of Prior Knowledge (PK) during optimization, and the implementation details of the chosen algorithms.

Joint optimization. Algorithm 1 illustrates the nested joint HPO applied in AutoPQ. The outer loop aims to identify the optimal hyperparameter configuration for the point

Algorithm 1 The AutoPQ HPO algorithm optimizes the hyperparameters of the point forecasting method and the sampling hyperparameter of the cINN jointly, taking into account the significantly lower computational effort of the latter.

Input: $\Lambda_p, \Lambda_q, B_i, B_t, \mathbf{X}_{\text{train}}, \mathbf{X}_{\text{val}}, y_{\text{train}}, y_{\text{val}}, f_{\text{cINN}}(\cdot)$

```

# Initialize Propulate [61] (EA)
1: trial_generator_p( $\Lambda_p$ )
2:  $b_t \leftarrow 0$  s
3: while  $b_t < B_t$  do
4:    $t \leftarrow \text{get\_current\_time}()$ 
5:    $\lambda_p \leftarrow \text{trial\_generator\_p.get\_config}()$ 
   # High computational effort
6:    $f_p(\cdot) \leftarrow \text{train\_p\_model}(\lambda_p, \mathbf{X}_{\text{train}}, y_{\text{train}})$ 
   # Distribution of  $\lambda_q^{\star}$  in active population
7:    $m, s \leftarrow \text{trial\_generator\_p.get\_stats}()$ 
   # Initialize Hyperopt [60] (BO) with PK
8:   trial_generator_q( $\Lambda_q, m, s$ )
9:   for  $b_i \leftarrow 0$  to  $B_i$  do
10:     $\lambda_q \leftarrow \text{trial\_generator\_q.get\_config}()$ 
    # Low computational effort
11:     $f_q(\cdot) \leftarrow \text{generate\_q\_model}(f_p(\cdot), f_{\text{cINN}}(\cdot), \lambda_q)$ 
    # Low computational effort
12:     $Q \leftarrow \text{assess\_performance}(f_q(\mathbf{X}_{\text{val}}, y_{\text{val}}))$ 
13:    trial_generator_q.update( $Q, \lambda_q$ )
14:     $b_i \leftarrow b_i + 1$ 
15:    if (early_stopping( $Q$ )) then
16:      break
17:    end if
18:  end for
19:   $\lambda_q^{\star} \leftarrow \text{trial\_generator\_q.get\_best\_config}()$ 
   # Store  $\lambda_q^{\star}$  associated with  $\lambda_p$ 
20:  trial_generator_p.update( $Q, \lambda_p, \lambda_q^{\star}$ )
21:   $b_t \leftarrow b_t + (\text{get\_current\_time}() - t)$ 
22: end while
23:  $\lambda_p^{\star}, \lambda_q^{\star} \leftarrow \text{trial\_generator\_p.get\_best\_config}()$ 

```

Output: $\lambda_p^{\star}, \lambda_q^{\star}$

Λ_p, Λ_q : configuration space (point forecast, quantile forecast); B_i, B_t : budget (iteration, time); $\mathbf{X}_{\text{train}}, \mathbf{X}_{\text{val}}$: model inputs (training, validation); $y_{\text{train}}, y_{\text{val}}$: model outputs (training, validation); $f_{\text{cINN}}, f_p, f_q$: trained model (cINN, point forecast, quantile forecast); $\lambda_p^{\star}, \lambda_q^{\star}$: optimal configuration (point forecast, quantile forecast)

forecasting method λ_p^* . First, the outer loop trial generator suggests a candidate λ_p . Importantly, after the random trial generator initialization, this suggestion is based on the probabilistic forecasting performance Q of previous trials and not on their point forecasting performance. Then, the point forecasting model $f_p(\cdot)$ is trained. Afterward, the inner loop optimizes the corresponding sampling hyperparameter λ_q^* by solving (5). Specifically, the inner loop trial generator proposes a candidate λ_q , and the quantile forecast $f_q(\cdot)$ is generated by passing the point forecast of $f_p(\cdot)$ forward through the cINN, generating samples from the point forecast’s latent space representation, and subsequently passing them backward through the cINN. Then, the probabilistic forecasting performance Q is assessed, and the inner loop generator is updated with Q and λ_q . The inner loop continues until an early stopping condition is met or the iteration budget B_i is exhausted, yielding the optimal sampling hyperparameter λ_q^* associated with λ_p . Before starting a new outer loop iteration, the outer trial generator is updated with the probabilistic forecasting performance Q , λ_p , and λ_q^* to suggest a new candidate λ_p for the point forecasting model. It continues until the time budget B_t is exhausted, ultimately yielding the optimal configuration, i. e., λ_p^* and the associated λ_q^* .⁶

Prior knowledge. In initializing the inner trial generator, we leverage PK by assuming that the optimal sampling hyperparameter λ_q^* for a given point forecasting method configuration λ_p is related to previously assessed configurations. Consequently, the inner trial generator begins with statistical parameters derived from these past configurations.⁷

Optimization algorithms. Since we do not have a closed-form expression of the configuration space Λ in (6) and the objective function Q is noisy, non-differentiable, and potentially non-convex, solving (6) requires black-box optimization methods. These methods serve as trial generators, suggesting new candidate configurations to be evaluated in both the inner and outer loop of Algorithm 1.

Training the point forecasting model in the **outer loop** is computationally expensive and benefits from GPU acceleration. Using multiple GPUs enables evaluating multiple hyperparameter configurations λ_p (i. e., multiple trials of Q) in parallel. To handle varying training durations and avoid GPU idle time, asynchronous optimization is applied. For this purpose, we employ the Python package `Propulate` [61] as the outer trial generator. This evolutionary optimizer maintains a continuous population for asynchronous configuration assessments⁸, which also enables incorporating PK into the inner loop.

Generating a probabilistic forecast based on a point forecast in the **inner loop** is computationally cheap. Additionally, leveraging PK enables rapid convergence, often resulting in early stopping. Hence, parallelizing the inner loop would add unnecessary overhead without reducing computation time. Instead, the inner loop runs sequentially using the Python package `Hyperopt` [60] as trial generator. `Hyperopt` employs BO with the TPE as the surrogate model to explore and exploit the configuration space by estimating the distribution of well-performing hyperparameter configurations in relation to underperforming ones [62]. To initialize `Hyperopt`, we use PK obtained from the outer loop trial generator `Propulate`. Specifically, the mean m and standard deviation s of the optimal sampling hyperparameters’ natural logarithms are computed from already assessed candidates in `Propulate`’s population (see Figure 3a). These values are then used to define `Hyperopt`’s prior distribution as $\log -\mathcal{N}(m, s)$. Assuming a log-normal distribution excludes negative values and is valid, as demonstrated in Figure 3a with the MLP on the Load-BW dataset. A random set of λ_q values is initially drawn from this prior distribution to explore regions with high prior probabilities before fitting the TPE surrogate model. Afterward, the fitted TPE is used to schedule new candidates of $\{\lambda_{q,0}, \lambda_{q,1}, \dots\}$ through an acquisition function that balances exploration and exploitation. Each assessed $\lambda_{q,i}$ (i. e., each trial of Q) updates the TPE surrogate model with its performance Q , reducing the prior distribution’s influence over iterations. Thus, values in regions with lower prior probabilities are also considered, unless early stopping occurs beforehand, as demonstrated in Figure 3b with the MLP on the Load-BW dataset.

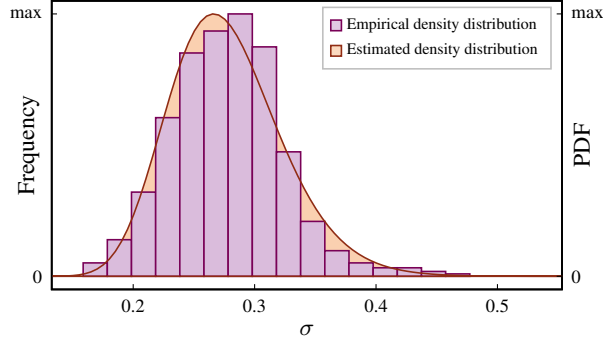
Early stopping. As with `AutoPQ-default`, optimization is stopped when the objective function’s value Q has converged or reached a satisfactory value. The inner loop is terminated if Q reaches a plateau across trials, i. e., the standard deviation of the five best-performing trials is less than 0.0005 with a patience of five trials.

Forecasting method selection. `AutoPQ-advanced` aims to select the best point forecasting method while jointly optimizing its hyperparameters λ_p and the corresponding sampling hyperparameter λ_q . To efficiently combine method selection and joint HPO, we use successive halving pruning. This method prunes underperforming configurations and re-allocates resources to more promising ones. Starting from the considered candidate forecasting methods, successive halving (Algorithm 2) iteratively eliminates the worst-performing methods and re-allocates resources to the better-performing ones, until one top candidate remains when the total time budget B_t is exhausted. Crucially, HPO for the remaining candidates continues from checkpoints of the previous pruning round, allowing optimization runs to be split over multiple HPC jobs.

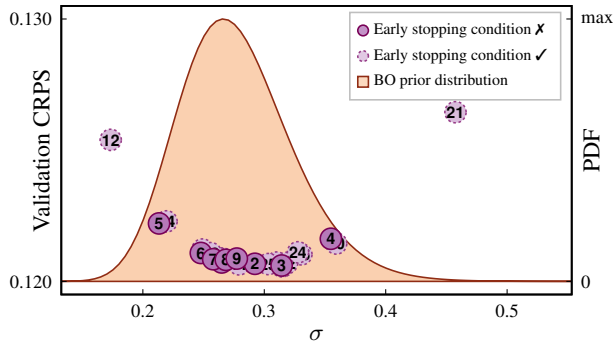
⁶The time budget refers to creating a model for one dataset.

⁷These values are stored during outer trial generator updates.

⁸The EA’s setup is based on [61] and detailed in Table A2 in the Appendix.



(a) Estimated BO prior distribution based on the optimal sampling hyperparameters associated and stored with the active and already assessed candidates of the EA population, visualized as empirical density distribution. We assume a log-normal distribution and estimate its expected value m and standard deviation s .



(b) Initializing the BO with the estimated prior distribution already provides a good estimate for the first trials, before the TPE surrogate model fitted on these trials gains influence. To illustrate the progression after the early stopping condition is met at the ninth iteration, the BO was continued until the 25th iteration (dashed dots), with each dot representing an iteration. After reaching this condition, sampling also continues at the edges of the distribution (iterations 12 and 21).

Figure 3: Estimated BO prior distribution and its utilization in the HPO of the sampling hyperparameter.

4 Evaluation

To evaluate AutoPQ⁹ comprehensively, we first assess its probabilistic forecasting performance with default and advanced configurations to analyze the impacts of HPO on improving the probabilistic performance. Second, we conduct an ablation study to evaluate the effectiveness of AutoPQ-advanced, which jointly optimizes the hyperparameters of the point forecaster and the cINN’s sampling hyperparameter. Third, we compare the computational efforts of AutoPQ-default and AutoPQ-advanced.

⁹A Python implementation of AutoPQ can be found on GitHub: <https://github.com/SMEISEN/AutoPQ>

Algorithm 2 The successive halving pruning strategy re-allocates computing resources from unpromising areas in the CASH configuration space to more promising ones.

Input: $\Lambda, B_t, \mathbf{X}_{\text{train}}, \mathbf{X}_{\text{val}}, \mathbf{Y}_{\text{train}}, \mathbf{Y}_{\text{val}}$

```

# Initialize result store
1: result_store( $\Lambda$ )
2: while len( $\Lambda$ ) > 1 do
3:   for  $\Lambda_i$  in  $\Lambda$  do
# Parallel evaluation, split computation budget
4:      $B_{t,i} \leftarrow B_t / \text{len}(\Lambda)$ 
# Initialize HPO algorithm with stored results
5:     hpo_algo(result_store)
# Run until budget is exhausted
6:     hpo_algo.run( $\Lambda_i, \mathbf{X}_{\text{train}}, \mathbf{X}_{\text{val}}, \mathbf{Y}_{\text{train}}, \mathbf{Y}_{\text{val}}, B_{t,i}$ )
7:      $Q_i^*, \lambda_i^* \leftarrow \text{hpo\_algo.get\_best\_config}(\Lambda_i)$ 
# Update result store
8:     result_store.update( $Q_i^*, \lambda_i^*$ )
9:   end for
# Shrink configuration space
10:   $\Lambda \leftarrow \text{result\_store.get\_best\_half}()$ 
11: end while

```

Output: λ^*

Λ : configuration space; B_t : time budget; $\mathbf{X}_{\text{train}}, \mathbf{X}_{\text{val}}$: model inputs (training, validation); $\mathbf{Y}_{\text{train}}, \mathbf{Y}_{\text{val}}$: model outputs (training, validation); λ^* : optimal configuration

4.1 Benchmarking

The subsequent section outlines the experimental setup for assessing probabilistic forecasting performance, followed by a presentation of the results and key insights gained from the analysis.

4.1.1 Experimental setup

In the following, we detail the data utilized, the evaluation strategy employed, and the benchmarks considered.

Data. AutoPQ is evaluated on six distinct datasets: Load-BW, Load-GCP, Mobility, Price, PhotoVoltaic (PV), and Wind Power (WP). Each dataset is briefly described below, followed by details on pre-processing and feature selection. Additional information is provided in Table A7 in the Appendix.

The **Load-BW** dataset [63] includes the gross electrical consumption of Baden-Württemberg, Germany, obtained from the Open Power System Data (OPSD) platform. The regional electrical consumption reflects the aggregation of a large number of Grid Connection Points (GCPs).

The **Load-GCP** dataset [64] contains the electrical consumption time series of 370 GCPs within a distribution grid in Portugal. The time series MT_158 is used to generate local forecasts, representing the local load of a single GCP.

The **Mobility** dataset [65] comprises hourly records of bike rentals in Washington D.C., USA, which serve as

an indicator of individual mobility within the smart grid context. Relevant weather and seasonal information such as air temperature, wind speed, and whether a day is a workday, weekend or holiday, are included.

The **Price** dataset features zonal electricity prices from an unspecified location, provided in the Global Energy Forecasting Competition (GEFCom) 2014 [66] price forecasting track. This challenge involved 14 tasks requiring day-ahead forecasts based on exogenous time series data, including total electrical consumption and zonal price. All 14 tasks are combined into one dataset for the evaluation.

The **PV** dataset includes the power generation of an Australian PhotoVoltaic (PV) plant, sourced from the GEFCom 2014 [66] PV power forecasting track. This track comprised 16 day-ahead forecasting tasks, supplemented by Numerical Weather Predictions (NWP) for the site from European Centre for Medium-Range Weather Forecasts (ECMWF), including Global Horizontal Irradiance (GHI) and cloud cover. For the evaluation, all 16 tasks are combined in one dataset.

The **WP** dataset contains the power generation of an Australian wind farm, taken from the GEFCom 2014 [66] Wind Power (WP) forecasting track. This track consisted of 16 day-ahead forecasting tasks, also with NWP for the site from ECMWF available, including wind speed and direction at a height of 10 m and 100 m. All 16 tasks are combined into one dataset for the evaluation.

Originally, all datasets considered are hourly resolved, except for the Load-GCP dataset, which was resampled to hourly resolution.

Evaluation strategy. We evaluate the day-ahead forecasting performance of AutoPQ on the six datasets described above, comparing both AutoPQ-`default` and AutoPQ-`advanced` configurations. To ensure comparability across the datasets, we normalize each dataset before creating separate training, validation, and test sub-sets.¹⁰ Detailed sample indices for these splits and selected exogenous features are provided in Table A7 in the Appendix.

We consider nine different point forecasting methods, choosing three from each method family: sARIMAX, ETS, and TBATS from SM; MLP, SVR, and XGB from ML; and DeepAR, N-HiTS, and TFT from DL. For AutoPQ-`default`, we train all nine methods with their default configurations $\lambda_{p,\text{default}}$, generate probabilistic forecasts from the point forecasts, and optimize the sampling hyperparameter λ_q for each model, where the best-performing one is selected afterward.¹¹ These results are compared to our evaluation of AutoPQ-`advanced`, which jointly optimizes

¹⁰For the forecasting methods MLP, DeepAR, N-HiTS, and TFT, 20% of the training dataset are hold-out for early stopping, i. e., the training process is terminated when the loss on the hold-out data increases.

¹¹The results of AutoPQ-`default` for the datasets Load-GCP, Mobility, Price, and PV are taken from [59], while the results for the additional datasets Load-BW and WP are not yet published.

both configurations, i. e., λ_p and λ_q , and applies CASH with the successive halving pruning strategy for the specified time budget of $B_t = 8$ h.

Two crucial properties in evaluating probabilistic forecasts are sharpness and calibration. According to Gneiting *et al.* [67], probabilistic forecasts should aim to maximize sharpness without negatively affecting the calibration. To balance these properties, the Continuous Ranked Probability Score (CRPS)

$$\text{CRPS} = \frac{1}{K} \sum_{k=1}^K \int_{\mathbb{R}} (\hat{F}_Y[k](x) - \mathbb{1}\{y[k] \leq x\})^2 dx, \quad (7)$$

is used as metric for both tuning and assessment, averaged over all time points K . In (7), $\hat{F}[k]$ is the estimated CDF of the forecast at time point k and the realized value $y[k]$ is translated into a degenerate distribution with the indicator function $\mathbb{1}\{y[k] \leq x\}$, which is one if $y[k]$ is less than the integration variable x , and zero otherwise.

The evaluation is performed five times on each dataset, with the arithmetic mean and the standard deviation reported to account for stochastic effects in training and optimization. We ensure consistent results using the same hardware for all runs.¹² Additionally, we report computing time and electricity consumption to quantify the computational effort and enable comparisons related to sustainability, as detailed in [25].

Benchmarks. We compare the probabilistic forecasting performance of AutoPQ against multiple benchmarks, categorized into two groups: direct probabilistic forecasts and probabilistic forecasts derived from existing point forecasts.¹³

The first category includes the direct probabilistic forecasts DeepAR, QRNNs, and the NNQF, which are detailed in Section 2. We implement DeepAR [26] using the Python package `PyTorch Forecasting` [68], the QRNNs with the Python package `Keras` [69] using the built-in `PL` function, and the NNQF [30] using the MLP of the `Scikit-learn` [70] Python package.

The second category includes the point forecast-based probabilistic forecasts Gaussian PIs, Empirical PIs, and Conformal PIs. While all of these methods consider the residuals $r[k] = |\hat{y}[k] - y[k]|$, $\forall k \in \mathbb{N}_1^{K_{\text{val}}}$ between the point forecasts $\hat{y}[k]$ and the realized values $y[k]$ from a validation dataset, they differ in their approach to calculate PIs. Gaussian PIs [14] assume Gaussian-distributed residuals and estimate the standard deviation σ to calculate PIs centered around the point forecast, adjusting σ

¹²Each run is performed with four parallel trials using two Intel Xeon Platinum 8368 Central Processing Units (CPUs) with 76 cores, four NVIDIA A100-40 GPUs with 40 GB memory (GPUs are utilized only for DL-based forecasting methods), and 256 GB Random-Access Memory (RAM), all provided by the HPC system HoreKa.

¹³The benchmark results for the datasets Load-GCP, Mobility, Price, and PV are taken from [59], while the results for the additional datasets Load-BW and WP are not yet published.

by a factor corresponding to the desired confidence level. In contrast, Empirical PIs [16] do not assume a specific parametric PDF but use the empirical PDF of residuals (i. e., sorting $r[k]$ from smallest to largest) to calculate PIs based on the desired confidence level. Conformal PIs for multi-step-ahead forecasts [17] calibrate the PIs for each forecast horizon without assuming a specific parametric PDF. A critical non-conformity score is calculated for each $r[k]$, and the temporal dependencies between these scores across the forecast horizon are obtained using Bonferroni correction. These corrected scores are used to calculate PIs centered around the point forecast.

For each point forecast-based probabilistic benchmark, we compare against the best-performing base forecast. That is, we select the point forecasting method achieving the lowest CRPS after calculating PIs using the Gaussian, the Empirical, and the Conformal approach, respectively.

4.1.2 Results

In the following, we summarize and visualize our benchmarking results, followed by an interpretation and discussion in Section 5.

Three key observations can be made from the benchmarking results in Table 2: First, and most importantly, AutoPQ-advanced shows a significant performance advantage over AutoPQ-default and other benchmarks. Second, the performance variability across datasets is greater for the direct probabilistic forecasting methods DeepAR, QRNNs, and NNQF compared to the point forecast-based probabilistic forecasting methods Gaussian, Empirical, and Conformal PIs as well as both AutoPQ-default and AutoPQ-advanced. Third, the average performance across datasets is lower for DeepAR, QRNNs, NNQF, and Gaussian PIs compared to Empirical PIs, Conformal PIs, AutoPQ-default, and AutoPQ-advanced.

Table 3 shows the percentage improvement of AutoPQ-advanced relative to the six benchmarks and AutoPQ-default per dataset. Improvements are highlighted with an asterisk if they are significant, i. e., the p-value of the one-tailed t-test is less than 0.05. The following insights can be drawn from the table: First, we observe significant improvements in 38 out of 42 tests (across seven methods and six datasets). Second, AutoPQ-advanced shows significant improvement over each direct probabilistic benchmark, averaging at least 15.1%, and each point forecast-based probabilistic benchmark, averaging at least 9.1%. Third, AutoPQ-advanced outperforms AutoPQ-default by 5.0% on average.

4.1.3 Insights

Figure 4 provides a visual comparison of PIs generated by AutoPQ-advanced using three exemplarily selected point forecasting methods (ETS, XGB, and TFT) compared to the probabilistic benchmarks for the Mobility dataset. The AutoPQ-advanced PIs are generated for the best-performing configuration identified through CASH with successive

halving, with TFT being the best method for this dataset (as detailed later in Figure 7). Figure 4 (a-c) shows that the PIs generated from the three point forecasting methods vary in sharpness, as reflected in their widths. Notably, clear differences are evident between the considered methods TFT, XGB, and ETS, ranking first, fourth, and ninth in the CASH, respectively.

Another observation concerns the PIs when the realized values are near zero or zero. Since the forecasted value (mobility indicator) is restricted to non-negative values, negative PIs are unreasonable. AutoPQ’s PIs account for this restriction, unlike the probabilistic benchmarks’ PIs, cf. Figure 4 (a-c) and (d-i). However, the post-processing required for AutoPQ’s quantiles to comply with this non-zero constraint on the CRPS is minimal, as detailed in Table A3 in the Appendix.

4.2 Ablation study

This section outlines the experimental setup of the ablation study, which evaluates the effectiveness of the automation methods applied in AutoPQ-advanced, followed by the presentation of results and insights.

4.2.1 Experimental setup

In the following, we outline the data used, the evaluation strategy employed, and the ablations considered in our experimental setup.

Data. As for benchmarking, the ablation study of AutoPQ-advanced is performed on six different datasets: Load-BW, Load-GCP, Mobility, Price, PV, and WP (see Section 4.1 for an overview).

Evaluation strategy. The ablation study is based on a similar evaluation strategy as the previous benchmarking. Specifically, the six datasets outlined in Section 4.1 are normalized and divided into training, validation, and test sets, as detailed in Table A7 in the Appendix.

To reduce the computational effort, we only consider the MLP and N-HiTS point forecasting methods without using successive halving. This selection is reasoned by i) the computational effort, ii) the probabilistic performance, and iii) the sensitivity to HPO. As illustrated in Figure 2, MLP and N-HiTS require low and moderate to high computational effort, respectively. In addition, both methods achieve competitive probabilistic performance and respond well to HPO, as shown later in Table 4.

In line with the benchmarking, the CRPS metric (7) is used for both tuning and assessment, with evaluations conducted five times on each dataset. To ensure consistent runtime measurements, we utilize the same hardware as for the benchmarking in all runs (see Section 4.1).

Ablation 1. The effectiveness of the inner loop in Algorithm 1, responsible for finding the optimal sampling

Table 2: The CRPS evaluated on the hold-out test sets with methods categorized into three groups: i) direct probabilistic benchmark methods, ii) point forecast-based probabilistic benchmark methods, and iii) AutoPQ with the default and the advanced configuration. The results of the benchmarks and AutoPQ-default for the datasets Load-GCP, Mobility, Price, and PV originate from [19].

	DeepAR	QRNNs	NNQF	Gaussian PIs	Empirical PIs	Conformal PIs	AutoPQ default	AutoPQ advanced
Load-BW	0.192 ± 0.008	0.145 ± 0.002	0.208 ± 0.004	0.156 ⁽¹⁾ ± 0.000	0.143 ⁽¹⁾ ± 0.000	0.143 ⁽¹⁾ ± 0.000	0.147 ⁽¹⁾ ± 0.001	0.138 ⁽¹⁾ ± 0.001
Load-GCP	0.312 ± 0.009	0.287 ± 0.002	0.263 ± 0.001	0.299 ⁽¹⁾ ± 0.000	0.234 ⁽¹⁾ ± 0.000	0.234 ⁽¹⁾ ± 0.000	0.234 ⁽¹⁾ ± 0.002	0.218 ⁽¹⁾ ± 0.001
Mobility	0.299 ± 0.007	0.443 ± 0.006	0.542 ± 0.004	0.360 ⁽²⁾ ± 0.021	0.268 ⁽²⁾ ± 0.015	0.268 ⁽²⁾ ± 0.015	0.263 ⁽²⁾ ± 0.004	0.258 ⁽²⁾ ± 0.005
Price	0.158 ± 0.005	0.157 ± 0.002	0.183 ± 0.003	0.279 ⁽²⁾ ± 0.008	0.161 ⁽²⁾ ± 0.005	0.161 ⁽²⁾ ± 0.005	0.140 ⁽²⁾ ± 0.006	0.131 ⁽³⁾ ± 0.001
PV	0.151 ± 0.013	0.101 ± 0.001	0.119 ± 0.000	0.208 ⁽¹⁾ ± 0.000	0.125 ⁽¹⁾ ± 0.000	0.125 ⁽¹⁾ ± 0.000	0.106 ⁽¹⁾ ± 0.001	0.101 ⁽¹⁾ ± 0.001
WP	0.618 ± 0.028	0.374 ± 0.002	0.394 ± 0.004	0.419 ⁽¹⁾ ± 0.000	0.373 ⁽¹⁾ ± 0.000	0.373 ⁽¹⁾ ± 0.000	0.377 ⁽¹⁾ ± 0.001	0.362 ⁽¹⁾ ± 0.001
Median	0.245	0.222	0.236	0.289	0.197	0.197	0.191	0.178
Mean	0.288	0.251	0.285	0.287	0.217	0.217	0.211	0.201

best-performing base point forecasting method: (1) XGB, (2) TFT, (3) N-HITS

Table 3: The percentage improvement of AutoPQ-advanced over the comparison methods in terms of the CRPS evaluated on the hold-out test data. AutoPQ-advanced uses HPO to optimize both the configuration of the point forecasting method λ_p and the cINN’s sampling hyperparameter λ_q , while AutoPQ-default only optimizes λ_q .

	DeepAR	QRNNs	NNQF	Gaussian PIs	Empirical PIs	Conformal PIs	AutoPQ default
Load-BW	28.1 % *	4.8 % *	33.7 % *	11.5 % ⁽¹⁾	3.5 % ⁽¹⁾	3.5 % ⁽¹⁾	6.1 % ⁽¹⁾
Load-GCP	30.1 % *	24.0 % *	17.1 % *	27.1 % ⁽¹⁾	6.8 % ⁽¹⁾	6.8 % ⁽¹⁾	6.8 % ⁽¹⁾
Mobility	13.7 % *	41.8 % *	52.4 % *	28.3 % ⁽²⁾	3.7 % ⁽²⁾	3.7 % ⁽²⁾	1.9 % ⁽²⁾
Price	17.1 % *	16.6 % *	28.4 % *	53.0 % ⁽²⁾	18.6 % ⁽²⁾	18.6 % ⁽²⁾	6.4 % ⁽²⁾
PV	33.1 % *	0.0 %	15.1 % *	51.4 % ⁽¹⁾	19.2 % ⁽¹⁾	19.2 % ⁽¹⁾	4.7 % ⁽¹⁾
WP	41.4 % *	3.2 % *	8.1 % *	13.6 % ⁽¹⁾	2.9 % ⁽¹⁾	2.9 % ⁽¹⁾	4.0 % ⁽¹⁾
Mean	27.3 %	15.1 %	25.8 %	30.8 %	9.1 %	9.1 %	5.0 %

* improvement is significant (p-value < 0.05); best-performing base point forecasting method: (1) XGB, (2) TFT

hyperparameter λ_q^* , is assessed. For comparison, a conventional HPO is used that does not take into account the different computational efforts required for training the point forecasting model and generating probabilistic forecasts. This is achieved by omitting the inner loop of Algorithm 1, resulting in Algorithm 3. In this setup, the trial generator suggests configurations for both the point forecaster λ_p and the sampling hyperparameter λ_q as combined configuration space $\lambda = \lambda_p \times \lambda_q$. Thus, only one sampling hyperparameter is assessed for each trained point forecasting model. To ensure comparability, both Algorithm 1 and 3 are run without successive halving, i. e., using the full time budget $B_t = 8$ h and considering the same configuration spaces.

Ablation 2. Different trial generators for the inner loop of Algorithm 1 are compared. Specifically, we compare PK-based BO against random search and BO, neither of which uses PK. The comparison is based on the number of iterations required to fulfill the early stopping condition outlined in Section 3.4.1. To avoid the computationally expensive task of repeating the entire CASH process for all six datasets five times across all nine forecasting methods, we limit the comparison to repeating only the inner loop of Algorithm 1. Thus, the inner loop is executed five times for each dataset using the best configuration for each forecasting method and evaluated with the two trial generators being compared.

Ablation 3. The decision quality of the successive halving is evaluated, specifically the impact of pruning under-

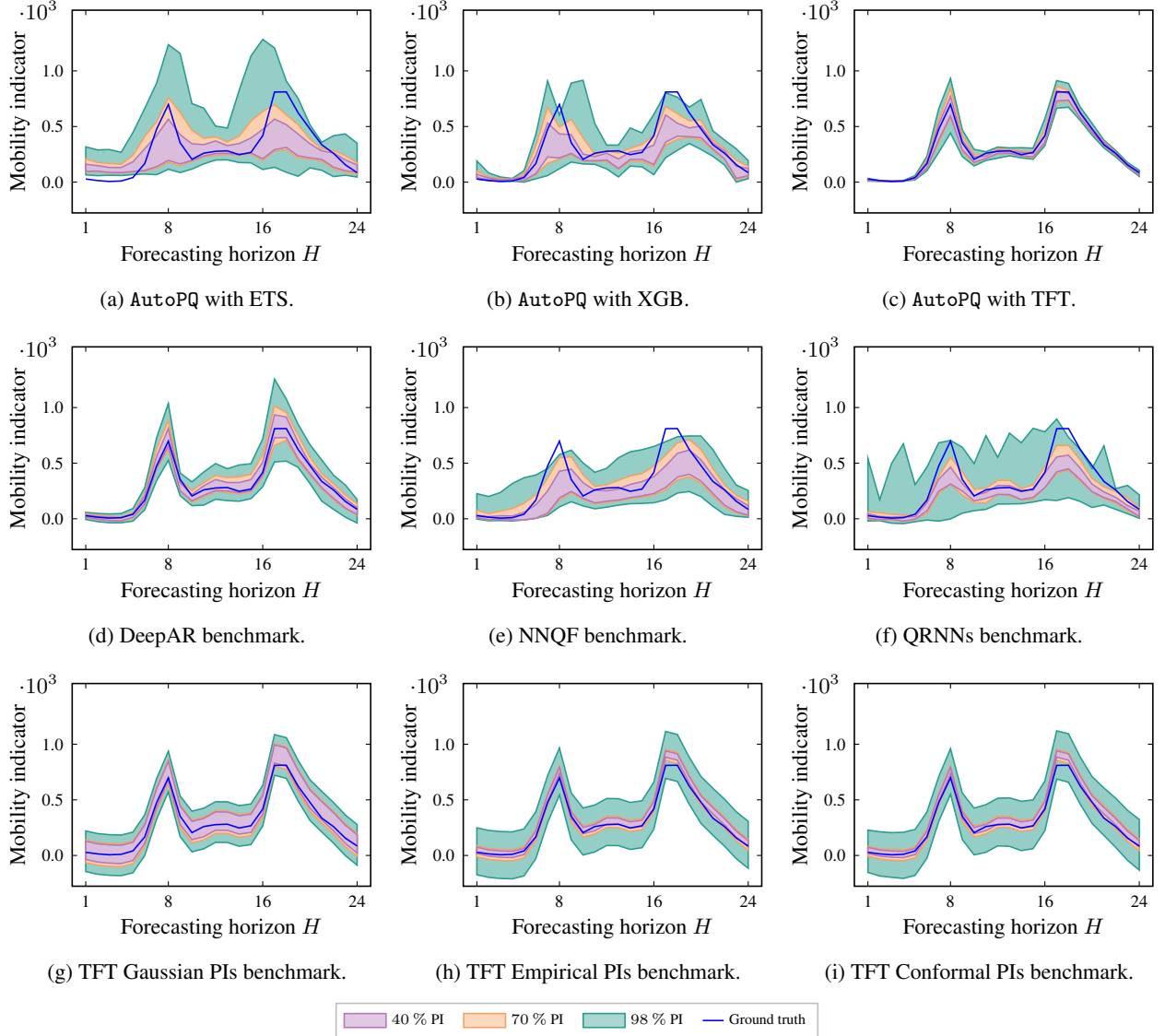


Figure 4: Exemplary 40 %, 70 %, and 98 % PIs for the Mobility dataset. The probabilistic forecasts of AutoPQ-advanced (a-c) are generated based on the point forecasting methods ETS (SM), XGB (ML), and TFT (DL), respectively, showing different performance. Note that AutoPQ-advanced automatically optimizes the hyperparameters and selects the best-performing method for each dataset, i. e., TFT for Mobility. The probabilistic benchmarks (d-i) can be categorized into direct probabilistic methods (DeepAR, NNQF, QRNNs) and point forecast-based probabilistic methods (Gaussian PIs, Empirical PIs, Conformal PIs based on a TFT forecaster).

performing forecasting methods in the CASH. To achieve this, we compare the evolution of the forecasting methods’ validation performances with successive halving to their performance evolution without pruning. Each pruned forecasting method from the benchmarking (see Section 4.1) is continued until the full time budget $B_t = 8$ h is exhausted. This allows us to analyze whether successive halving retains forecasting methods that ultimately perform well while pruning those that do not improve with additional computational effort. Additionally, we evaluate how the nine forecasting methods respond to HPO, i. e., the

improvement over the point forecasting methods’ default hyperparameter configurations.

4.2.2 Results

The following section summarizes the results of the ablation study and provides supporting visualizations, which are further interpreted and discussed in Section 5.

Ablation 1. The results comparing the effectiveness of the originally proposed AutoPQ HPO Algorithm 1 to its ablated version Algorithm 3 are presented in Figure 5 for

Algorithm 3 HPO algorithm for optimizing the point forecasting method’s hyperparameters and the cINN’s sampling hyperparameter simultaneously without considering the significantly lower computational effort of the latter.

Input: $\Lambda_p, \Lambda_q, B_t, B_t, \mathbf{X}_{\text{train}}, \mathbf{X}_{\text{val}}, \mathbf{y}_{\text{train}}, \mathbf{y}_{\text{val}}, f_{\text{cINN}}(\cdot)$

```

# Initialize Propagate [61] (EA)
1: trial_generator( $\Lambda_p, \Lambda_q$ )
2:  $b_t \leftarrow 0$ s
3: while  $b_t < B_t$  do
4:    $t \leftarrow \text{get\_current\_time}()$ 
5:    $\lambda_p, \lambda_q \leftarrow \text{trial\_generator.get\_config}(\Lambda_p, \Lambda_q)$ 
   # High computational effort
6:    $f_p(\cdot) \leftarrow \text{train\_p\_model}(\lambda_p, \mathbf{X}_{\text{train}}, \mathbf{y}_{\text{train}})$ 
   # Low computational effort
7:    $f_q(\cdot) \leftarrow \text{generate\_q\_model}(f_p(\cdot), f_{\text{cINN}}(\cdot), \lambda_q)$ 
   # Low computational effort
8:    $Q \leftarrow \text{assess\_performance}(f_q(\mathbf{X}_{\text{val}}, \mathbf{y}_{\text{val}}))$ 
9:   trial_generator.update( $\lambda_p, \lambda_q, Q$ )
10:   $b_t \leftarrow b_t + (\text{get\_current\_time}() - t)$ 
11: end while
12:  $\lambda_p^*, \lambda_q^* \leftarrow \text{trial\_generator.get\_best\_config}(\Lambda_p, \Lambda_q)$ 

```

Output: λ_p^*, λ_q^*

Λ_p, Λ_q : configuration space (point forecast, quantile forecast); B_t, B_t : budget (iteration, time); $\mathbf{X}_{\text{train}}, \mathbf{X}_{\text{val}}$: model inputs (training, validation); $\mathbf{y}_{\text{train}}, \mathbf{y}_{\text{val}}$: model outputs (training, validation); $f_{\text{cINN}}, f_p, f_q$: trained model (cINN, point forecast, quantile forecast); λ_p^*, λ_q^* : optimal configuration (point forecast, quantile forecast)

the MLP and N-HiTS. These figures exemplarily illustrate the CRPS evolution on the validation dataset over the HPO budget. The time budget marks for the pruning rounds are also shown to contextualize the validation performance within successive halving. We can draw two key observations from these figures: First, the mean value of Algorithm 1 is consistently lower than that of Algorithm 3 for most of the HPO time budget. Second, the mean value of Algorithm 1 is notably lower than that of Algorithm 3 at the beginning of the HPO. This gap narrows toward the end of the HPO time budget, with both values appearing to converge to the same value.¹⁴

Ablation 2. Figure 6 compares the results of different trial generators for the inner loop in Algorithm 1. The figure shows the number of iterations required until the early stopping condition is met, aggregated over all nine forecasting methods, the six datasets, and five runs.¹⁵ Three key observations emerge: First, BO using the TPE surrogate model significantly reduces the number of iterations compared to random search. Second, integrating PK into BO-TPE further decreases the number of required iterations. Notably, even the upper outliers fall within the range of the lower whisker of BO-TPE without PK. Third, all three trial generators achieve similar validation CRPS, as detailed in Table A8 in the Appendix. Specifically, BO-

TPE-PK delivers similar probabilistic performance while requiring significantly fewer iterations compared to the other two generators.

Ablation 3. Figure 7 shows the results of the successive halving ablation study.¹⁶ Three key findings are notable: First, the best-performing forecasting method remains consistent across all datasets, meaning it is not erroneously deactivated during pruning. Second, this best-performing method is already identified by AutoPQ-default. Rank changes occur among the following methods during successive halving. Third, while SM methods show significant improvements in the first pruning round (AutoPQ-advanced) compared to their default configuration (AutoPQ-default), they still rank last even with additional time budget. In contrast, the middle and upper ranks are competitive among methods from the ML and DL families.

4.2.3 Insights

Figure 8 illustrates the impact of leveraging PK for BO-TPE on each dataset. The plots depict the CRPS on the validation dataset together with the prior distribution over the sampling hyperparameter σ for both BO-TPE with and without PK. For BO-TPE, a continuous uniform PDF $\mathcal{U}(0, 3)$ is assumed, while BO-TPE-PK uses a log-normal PDF $\mathcal{N}(\mu, \sigma)$ with the parameters derived from the EA population. The PDFs in Figure 8 are normalized to their maximum value to ensure visual comparability. These plots, while only exemplarily showing the sampling hyperparameter optimization for the XGB point forecast, are representative of other point forecasting methods concerning the following observations: First, the optimal sampling hyperparameter $\lambda_q^* = \sigma^*$ is highly dependent on the dataset, showing differences in both location and sensitivity. For instance, the validation CRPS valley in Figure 8b is flatter than the one in Figure 8a. Correspondingly, the prior distribution of BO-TPE-PK shows varying spread. Second, Figure 8 confirms our earlier findings that BO-TPE-PK requires significantly fewer iterations to meet the early stopping condition. This condition is often satisfied before the TPE surrogate model starts trading off exploitation and exploration.

Examining the improvement in the validation CRPS without pruning as shown in Figure 7, we can calculate the percentage improvement. Results are listed in Table 4, where significant improvements with a p-value of the one-tailed t-test smaller than 0.05 are highlighted with an asterisk. Three observations stand out: First, the SM methods show inconsistent improvements; some exhibit large and significant enhancements, while others demonstrate little to no improvement. Second, the ML methods achieve significant improvements, with the MLP showing the best response to HPO, improving on average by 12.3%. Third, the DL methods achieve significant improvements only for DeepAR and N-HiTS, with average enhancements by

¹⁴Both observations also hold for the other four datasets and both of the considered forecasting methods.

¹⁵The computational effort scales approximately linearly with the number of iterations since the initialization effort is negligible.

¹⁶Figure 7 shows the representative results of run no. 1.

14.7% and 15.8%, respectively. In contrast, the TFT exhibits a weak response to HPO, showing no significant improvement in five of the six datasets.

4.3 Electricity consumption-awareness

Our benchmarking results demonstrate that AutoPQ-advanced can significantly enhance performance compared to AutoPQ-default. Since this improvement incurs a higher computational effort, the following evaluation aims to increase the awareness for energy-intensive performance improvements.

4.3.1 Experimental setup

Our evaluation is based on the average computational effort across the six datasets used in the benchmarking (Section 4.1). We measure the computational effort in terms of the electricity consumption because it is independent of data-center-specific or geopolitical factors at the time of collection [25].¹⁷ Since the research-exclusive HPC system HoreKa¹⁸ was used for benchmarking, we additionally estimate the monetary costs that would be incurred by the Amazon AWS cloud computing service with equivalent hardware.

4.3.2 Results

The following section summarizes the electricity consumption required for performance improvements and corresponding monetary costs, which are further interpreted and discussed in Section 5.

Electricity consumption. Figure 9 shows the total computing time and the corresponding electricity consumption of AutoPQ-default and AutoPQ-advanced required for a single run, averaged across datasets and runs.

While a single AutoPQ-default run uses 4.22 h of compute time and consumes 0.57 kWh of electrical energy, AutoPQ-advanced requires 81.78 h and consumes 8.73 kWh for a run, with $N_p = 9$ considered point forecasting methods and a time budget $B_t = 8$ h. This increased resource usage is due to the parallelized CASH, which evaluates four trial configurations simultaneously for each point forecasting method. As a result, the total computing time accumulates over all pruning rounds of successive halving. Specifically, the total computing time is calculated as the product of the number of active forecasting methods per round, the time budget per round, and the number of parallel trials conducted.

The benchmarking shows that the three SM point forecasting methods perform significantly worse than the ML- and DL-based methods. Omitting SM methods due to their weak performance, i. e., $N_p = 6$, would reduce the computational effort to 69.33 h and 7.75 kWh.

¹⁷Other metrics based on electricity consumption like the carbon footprint can be calculated using assumed or local conditions.

¹⁸<https://www.nhr.kit.edu/userdocs/horeka/>

The ablation study reveals that the performance of AutoPQ-default, which uses default hyperparameters for the point forecasting methods $\lambda_{p,\text{default}}$ with an optimized sampling hyperparameter λ_q^* , reflects the potential performance improvements achievable through HPO to identify λ_p^* with AutoPQ-advanced. Thus, AutoPQ-default can be viewed as the initial pruning round in the successive halving-based CASH of AutoPQ-advanced. Since the performance gains in the final pruning round are minimal, the overall time budget could be further reduced to $B_t = 4$ h. Both adjustments would decrease the computational effort to 30.89 h and 3.47 kWh.

Monetary costs. We calculate the monetary costs of using Amazon AWS for both AutoPQ-default and AutoPQ-advanced, based on equivalent hardware on the Amazon EC2 G4 instances [71]. For AutoPQ-advanced, the four-GPU instance g4ad.16xlarge (3.468 \$/h on demand) closely matches the hardware utilized on the HoreKa HPC system. Since four trials are evaluated in parallel, the billed computing time shown in Figure 9 is reduced by a factor of four. As the HPO of the sampling hyperparameter is performed sequentially for AutoPQ-default, the single-GPU instance g4ad.4xlarge (0.867 \$/h on demand) is comparable to the hardware utilized on HoreKa.

The costs for employing AutoPQ-default and AutoPQ-advanced on the above Amazon EC2 G4 instances are summarized in Table 5. Using AutoPQ-default would cost 3.66 \$, while using AutoPQ-advanced would cost 26.78 \$ with the electricity consumption-aware configuration ($N_p = 6$, $B_t = 4$ h). For simplicity, we assume that all forecasting methods utilize GPU instances, even though only the three DL methods benefit from them. To optimize costs and avoid GPU idle time, CPU-only instances should be employed for SM and ML point forecasting methods, as used for the benchmarking on HoreKa.

5 Discussion

The subsequent section discusses the results of the benchmarking, the ablation studies, as well as limitations and benefits.

5.1 Benchmarking

We discuss two aspects of the benchmarking results for probabilistic day-ahead forecasting performance across the six datasets: First, we observe a greater performance variability among the direct forecasting methods, i. e., DeepAR, QRNNs, and NNQF, compared to the point forecast-based probabilistic forecasting methods, i. e., Gaussian, empirical, and conformal PIs, as well as AutoPQ-default and AutoPQ-advanced. The reduced variability in the latter group can be attributed to the probabilistic forecast being based on multiple point forecasting methods, from which the best-performing method is selected.

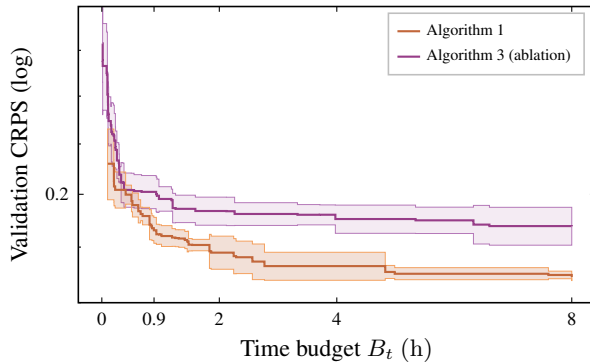
Table 4: The percentage improvement of each optimized configuration over the corresponding default configuration in the successive halving ablation study without pruning in terms of the CRPS evaluated on the validation data.

	ETS	sARIMAX	TBATS	MLP	SVR	XGB	DeepAR	N-HiTS	TFT
Load-BW	57.7% *	12.9% *	0.5%	29.2% ⁽³⁾	0.3%	7.5% ⁽¹⁾	25.6% *	30.5% ⁽²⁾	23.5% *
Load-GCP	<0.1%	<0.1%	8.0%	6.6% *	4.1% ⁽³⁾	4.8% ⁽¹⁾	16.7% *	4.8% *	6.7% ⁽²⁾
Mobility	42.3% *	40.5% *	45.0% *	4.9% *	4.4% *	6.8% *	8.9% ⁽²⁾	14.2% ⁽³⁾	1.0% ⁽¹⁾
Price	2.2%	52.5% *	<0.1%	8.9% ⁽²⁾	2.3% *	2.5% *	7.9% *	13.7% ⁽¹⁾	5.3% ⁽³⁾
PV	37.5% *	14.3%	56.7% *	10.2% ⁽³⁾	4.3% ⁽²⁾	6.2% ⁽¹⁾	13.8% *	22.0% *	6.9%
WP	<0.1%	<0.1%	<0.1%	13.9% ⁽³⁾	3.6% ⁽²⁾	5.6% ⁽¹⁾	15.0% *	9.3% *	8.5%

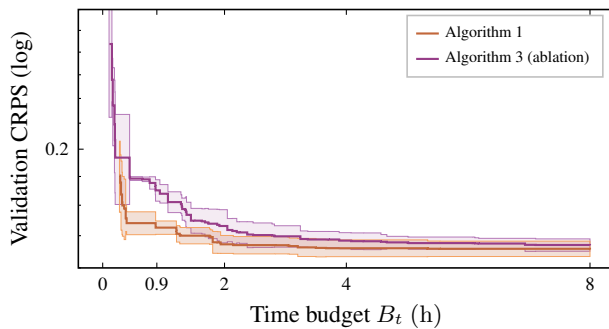
* improvement is significant (p-value < 0.05); (1), (2), (3): rank number in successive halving

Table 5: The monetary costs of using the Amazon EC2 G4 instances with hardware similar to the HoreKa HPC system.

AutoPQ configuration	Default	Advanced	Advanced	Default & Advanced
Point forecasting methods	$N_p = 9$	$N_p = 9$	$N_p = 6$	$N_p = 6$
Successive halving budget	-	$B_t = 8$ h	$B_t = 4$ h	$B_t = 4$ h
Amazon EC2 G4 instance	g4ad.4xlarge	g4ad.16xlarge	g4ad.16xlarge	g4ad.16xlarge
On-demand price	0.87 \$/h	3.47 \$/h	3.47 \$/h	3.47 \$/h
Computing hours	4.22 h	20.45 h	17.33 h	7.72 h
Monetary costs	3.66 \$	70.9 \$	60.11 \$	26.78 \$



(a) Convergence of MLP on Price.



(b) Convergence of N-HiTS on Price.

Figure 5: Comparison of the convergence of Algorithm 1 and 3 (ablation) for the HPO of the MLP and N-HiTS on the two exemplary datasets. The thick solid line represents the mean value, and the opaque area is the standard deviation over five runs.

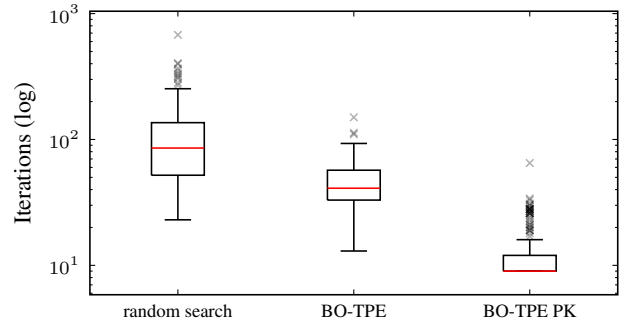
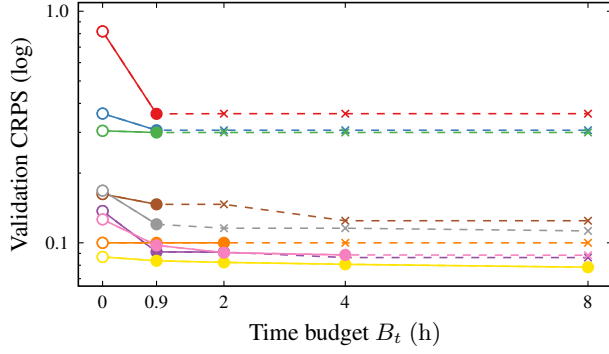
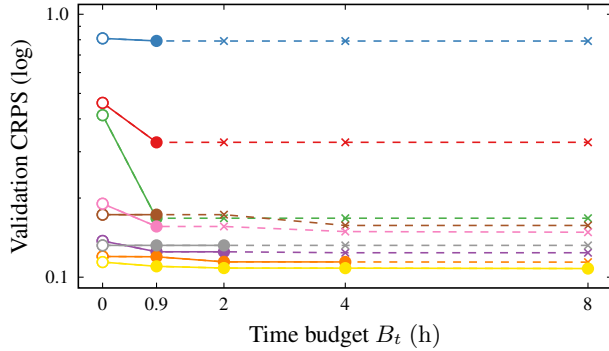


Figure 6: Number of iterations required for the inner loop of Algorithm 1 until the early stopping criterion is fulfilled, compared for three trial generators: random search, BO-TPE, and BO-TPE-PK. The box plot considers all nine forecasting methods, the six datasets, and five runs, i. e., 270 data tuples per trial generator.

This performance-based selection ensures that only the top method prevails, thus mitigating the risk of poor performance associated with any method underperforming on the dataset. Second, AutoPQ-advanced consistently outperforms AutoPQ-default and all benchmarking methods. Specifically, the average improvement of AutoPQ-advanced surpasses that of AutoPQ-default when compared to both direct probabilistic benchmarks and point forecast-based probabilistic benchmarks. This improvement is significant for five of the six datasets, suggesting that AutoPQ-advanced is particularly well-suited for performance-critical smart grid applications subject to high decision costs.



(a) Successive halving pruning rounds on Load-BW.



(b) Successive halving pruning rounds on PV.



Figure 7: Evolution of the considered forecasting methods’ validation performances in the successive halving-based CASH of AutoPQ-advanced. The performance at 0h reflects AutoPQ-default, shown as a reference and thus not included in the time budget B_t . Solid lines with dot markers show the performance of active methods, while dotted lines with cross markers show the performance of inactive methods as it would have evolved without pruning. For simplicity, the progress in the successive halving pruning rounds is assumed to be linear.

5.2 Ablation study

Our results of the ablation study reveal three key points: First, the performance advantage of Algorithm 1 over Algorithm 3, evident at the beginning of the HPO, is decisive for the effectiveness successive halving. Since Algorithm 3 (ablation) risks prematurely pruning forecasting methods that could potentially perform well, its performance deficit is particularly high for the initial and subsequent pruning rounds. This is because the EA requires several generations to identify a suitable sampling hyperparameter, with random initialization potentially yielding both suitable and unsuitable parameters. In contrast, Algorithm 1 effectively identifies the optimal sampling hyperparameter for each

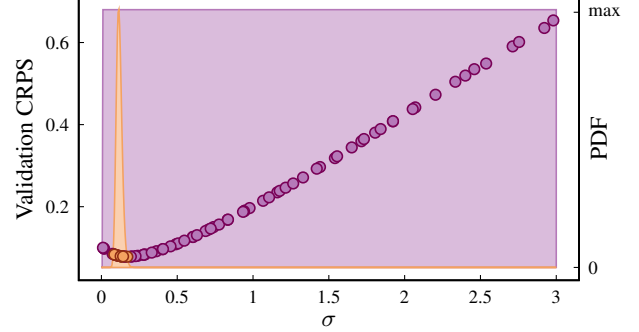
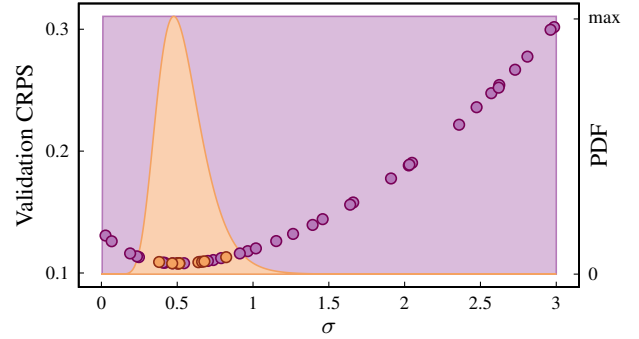
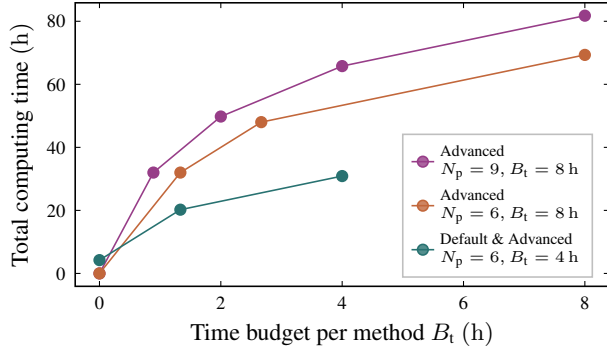
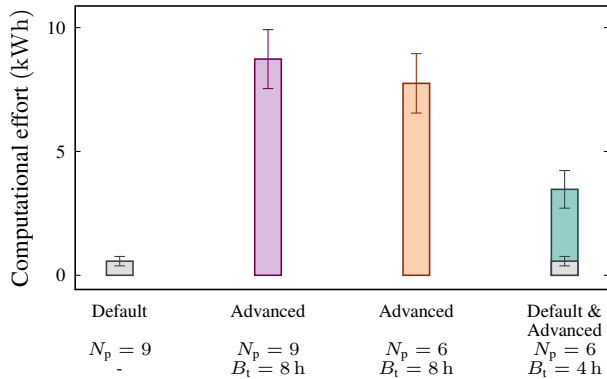
(a) λ_q -HPO on Load-BW.(b) λ_q -HPO on PV.

Figure 8: The HPO of the sampling hyperparameter conducted in the inner loop of Algorithm 1 using BO-TPE and BO-TPE-PK. The validation performance (CRPS) over the trial configurations (λ_q) is represented as dots, and the TPE prior distribution is shown as a filled area normalized by the maximum of the respective PDF. The plots illustrate the HPO for a single XGB configuration but are representative of the other point forecasting methods.

trained model, thereby reducing this variability. We observe this benefit for both N-HiTS (moderate to high computational effort) and the MLP (low computational effort), demonstrating the general effectiveness of Algorithm 1 across different forecasting methods. Second, leveraging PK for the inner loop trial generator significantly reduces the number of iterations. Maintaining a low iteration count is crucial for achieving the performance advantage of Algorithm 1 over Algorithm 3 (ablation). This improvement stems from the fact that the inner loop’s effectiveness relies on keeping the computational effort needed to identify the optimal sampling hyperparameter low compared to the time required to train the model. Third, successive halving proves effective in both pruning underperforming forecasting methods and retaining promising ones. We find that the three SM methods consistently perform poorly across all datasets and lag far behind ML and DL methods. Therefore, we recommend to exclude these methods to reduce the computational effort. For ML and DL methods, the



(a) Evolution of the total computing time.



(b) Resulting total electricity consumption.

Figure 9: Comparison of the computational effort for a run of AutoPQ-default and AutoPQ-advanced for different numbers of point forecasting methods N_p in the CASH and different time budgets B_t in the successive halving pruning strategy. Since AutoPQ-advanced assesses four trial configurations in parallel while AutoPQ-default runs sequentially, we multiply the total computing time of AutoPQ-advanced by four. The total electricity consumption was recorded by the HoreKa HPC system.

performance of their default hyperparameter configuration already provides a strong indicator of the method’s potential for performance improvement in the HPO. Thus, if one method significantly outperforms another using default configurations, this performance gap is unlikely to change substantially through HPO.

5.3 Electricity consumption-awareness

In the context of electricity consumption-awareness in view of sustainability, AutoPQ offers two configurations tailored to accommodate varying computing systems and performance needs: AutoPQ-default for general-purpose computing systems, delivering high-quality probabilistic forecasts, and AutoPQ-advanced, which necessitates HPC systems to enhance forecasting quality further. The latter uses a built-in successive halving strategy for optimizing resource use by pruning underperforming configurations and re-allocating computational resources to more promis-

ing ones. We recommend running AutoPQ-default first and using the model if the forecasting quality is satisfactory. Otherwise, the results can be used to initialize the successive halving-based CASH of AutoPQ-advanced, which can improve the CRPS up to 6.8%. In terms of the efforts required for performance improvements, we quantify the energy footprint and monetary costs of both AutoPQ-default and AutoPQ-advanced. Given that the monetary costs are relatively low compared to the personnel expenses associated with an iterative manual design process, we conclude that both AutoPQ-default and AutoPQ-advanced are cost-effective for most smart grid applications. For applications in which decision-making heavily relies on forecasting quality, we anticipate that AutoPQ-advanced will quickly amortize its higher initial costs, ultimately becoming more cost-efficient than AutoPQ-default in the long run.

5.4 Limitations

With regard to the limitations of AutoPQ, two key aspects are discussed: possibly untapped potential for further performance improvements and desirable probabilistic properties.

Possibly untapped performance improvement potential. Performance could be further improved through the configuration space design, the feature selection, and integrating PK. An improperly sized configuration space may either waste computational resources on insensitive hyperparameters or overlook sensitive hyperparameters, missing potential performance gains. While a comprehensive sensitivity analysis across various datasets is impractical due to high computational costs, AutoPQ’s configuration space design is based on best practices. Specifically, the hyperparameters and their value ranges are chosen according to recommendations provided in the respective forecasting methods’ documentation. The feature selection for the evaluation is based on [19] (AutoPQ-default) to ensure comparability in benchmarking. However, automated selection is preferable for real-world applications. This limitation could be addressed by using automated feature selection methods, e. g., the Minimum Redundancy Maximum Relevance (MRMR) filter method [72].

Desirable probabilistic properties. The benchmarking demonstrates that AutoPQ can be optimized to effectively minimize CRPS. Moreover, our previous work [59] highlights that optimizing the sampling hyperparameter for a customized metric allows the forecast to be tailored to different probabilistic properties. However, it remains unclear which probabilistic properties should be prioritized for specific real-world smart grid applications. This gap could be addressed by directly measuring the so-called forecast value of a configuration within the application, rather than relying on a probabilistic metric as a proxy. For instance, the forecast value could be assessed by using the resulting costs in a forecast-based electricity cost optimization prob-

lem, as shown in [73].¹⁹ This approach enables the HPO to assess how well the resulting probabilistic properties align with the application’s needs, rather than relying on a chosen probabilistic metric as a proxy.

5.5 Benefits

AutoPQ’s ability to automatically design high-quality probabilistic forecasts with tailored properties is essential for scaling smart grid applications. With the cost-effectiveness of training AutoPQ-advanced, we anticipate a swift return on investments for many smart grid applications, particularly where forecast quality is critical for decision-making. A key advantage of our approach is its versatility: the cINN can generate quantiles or PIs for any point forecasting method. This flexibility enables the integration of new forecasting methods into AutoPQ’s CASH process, while consistently removing underperforming point forecasting methods. Moreover, the joint optimization of the point forecasting methods’ hyperparameters and the cINN’s sampling hyperparameter is not limited to mathematically derivable validation metrics. This is crucial because it supports the use of any metrics for the assessment in the HPO process, including customized metrics or direct measurements of the so-called forecast value within smart grid applications, as previously suggested.

6 Conclusion and outlook

Designing probabilistic time series forecasting models for smart grid applications includes several challenges, i. e., i) quantifying forecast uncertainty in an unbiased and accurate manner, ii) automating the selection and enhancement of forecasting models to meet application needs, and iii) quantifying the environmental impacts required for performance improvements in view of sustainability.

In order to address these challenges, we introduce AutoPQ, a novel method for generating probabilistic forecasts. AutoPQ uses a cINN to convert point forecasts into quantile forecasts, leveraging existing well-designed point forecasting methods. AutoPQ automates the selection and optimization of these methods, ensuring the best model is chosen and fine-tuned to improve probabilistic forecasting performance. To handle varying performance needs and available computing power, AutoPQ comes with two configurations: the default configuration suitable for providing high-quality probabilistic forecasts on general-purpose computing systems, and the advanced configuration for further enhancing forecast quality on HPC systems.

The evaluation demonstrates that AutoPQ is both cost-effective and scalable, with significant performance improvements in forecasting quality over existing direct probabilistic forecasting benchmarks, averaging at least 15.1 %, and point forecast-based probabilistic benchmarks, av-

¹⁹In this study, several MLP-based point forecasting models are trained using different loss functions, and the model with the highest forecast value is selected.

eraging at least 9.1 %. Additionally, the evaluation addresses environmental concerns by assessing AutoPQ’s strategies for saving computing resources. Specifically, the energy consumption can be reduced by 60 % by adjusting AutoPQ-advanced’s successive halving strategy based on the ablation study results (omit SM methods, reduce time budget, and use AutoPQ-default as initial pruning round). Furthermore, information on AutoPQ’s electricity consumption and monetary costs required for performance improvements is reported. Specifically, the average improvement in forecast quality of 5 % of AutoPQ-advanced over AutoPQ-default additionally consumes 2.9 kWh and additionally costs 23.12 \$.

Future work will focus on refining the feature selection of AutoPQ, and incorporating the forecast value as the assessment metric to tailor the forecast directly to the application’s needs, rather than using a probabilistic metric like the CRPS as a proxy.

Acknowledgments

This project is funded by the Helmholtz Association under the Program “Energy System Design”, the Helmholtz Association’s Initiative and Networking Fund through Helmholtz AI, and was performed on the HoreKa supercomputer funded by the Ministry of Science, Research and the Arts Baden-Württemberg and by the Federal Ministry of Education and Research.

Conceptualization and methodology: S. M., K. P.; Literature review: S. M., K. P.; Data curation: K. P.; Formal analysis: S. M.; Structure: S. M.; Visualization and layout: S. M.; Writing – original draft preparation: S. M.; Writing – review and editing: S. M., K. P., O. T., M. W., M. G., R. M., V. H.; Supervision and funding acquisition: M. G., R. M., V. H.; All authors have read and agreed to the published version of the article.

References

- [1] H. Khajeh and H. Laaksonen, “Applications of probabilistic forecasting in smart grids: A review,” *Applied Sciences*, vol. 12, no. 4, 2022, ISSN: 2076-3417. DOI: 10.3390/app12041823.
- [2] T. Summers, J. Warrington, M. Morari, and J. Lygeros, “Stochastic optimal power flow based on conditional value at risk and distributional robustness,” *International Journal of Electrical Power & Energy Systems*, vol. 72, pp. 116–125, 2015, The Special Issue for 18th Power Systems Computation Conference., ISSN: 0142-0615. DOI: 10.1016/j.ijepes.2015.02.024.
- [3] R. Mieth and Y. Dvorkin, “Data-driven distributionally robust optimal power flow for distribution systems,” *IEEE Control Systems Letters*, vol. 2, no. 3, pp. 363–368, 2018.

- [4] R. R. Appino, J. Á. González Ordiano, R. Mikut, T. Faulwasser, and V. Hagenmeyer, “On the use of probabilistic forecasts in scheduling of renewable energy sources coupled to storages,” *Applied Energy*, vol. 210, pp. 1207–1218, 2018, ISSN: 0306-2619. DOI: 10.1016/j.apenergy.2017.08.133.
- [5] S. Henni, J. Becker, P. Staudt, F. vom Scheidt, and C. Weinhardt, “Industrial peak shaving with battery storage using a probabilistic forecasting approach: Economic evaluation of risk attitude,” *Applied Energy*, vol. 327, p. 120 088, 2022, ISSN: 0306-2619. DOI: 10.1016/j.apenergy.2022.120088.
- [6] K. Phipps, K. Schwenk, B. Briegel, R. Mikut, and V. Hagenmeyer, “Customized uncertainty quantification of parking duration predictions for EV smart charging,” *IEEE Internet of Things Journal*, vol. 10, no. 23, pp. 20 649–20 661, 2023. DOI: 10.1109/JIOT.2023.3299201.
- [7] J. Huber, D. Dann, and C. Weinhardt, “Probabilistic forecasts of time and energy flexibility in battery electric vehicle charging,” *Applied Energy*, vol. 262, p. 114 525, 2020, ISSN: 0306-2619. DOI: 10.1016/j.apenergy.2020.114525.
- [8] Y. Zhang, C. Cheng, R. Cao, G. Li, J. Shen, and X. Wu, “Multivariate probabilistic forecasting and its performance’s impacts on long-term dispatch of hydro-wind hybrid systems,” *Applied Energy*, vol. 283, p. 116 243, 2021, ISSN: 0306-2619. DOI: 10.1016/j.apenergy.2020.116243.
- [9] J. Han, L. Yan, and Z. Li, “A task-based day-ahead load forecasting model for stochastic economic dispatch,” *IEEE Transactions on Power Systems*, vol. 36, no. 6, pp. 5294–5304, 2021. DOI: 10.1109/TPWRS.2021.3072904.
- [10] B. N. Oreshkin, D. Carpov, N. Chapados, and Y. Bengio, “N-BEATS: Neural basis expansion analysis for interpretable time series forecasting,” in *International Conference on Learning Representations*, 2020.
- [11] B. Lim, S. Ö. Arık, N. Loeff, and T. Pfister, “Temporal Fusion Transformers for interpretable multi-horizon time series forecasting,” *International Journal of Forecasting*, vol. 37, no. 4, pp. 1748–1764, 2021, ISSN: 0169-2070. DOI: 10.1016/j.ijforecast.2021.03.012.
- [12] C. Challú, K. G. Olivares, B. N. Oreshkin, F. Garza Ramirez, M. Mergenthaler Canseco, and A. Dubrawski, “N-HiTS: Neural hierarchical interpolation for time series forecasting,” in *Proceedings of the AAAI Conference on Artificial Intelligence*, vol. 37, 2023, pp. 6989–6997. DOI: 10.1609/aaai.v37i6.25854.
- [13] F. Petropoulos *et al.*, “Forecasting: Theory and practice,” *International Journal of Forecasting*, vol. 38, no. 3, pp. 705–871, 2022, ISSN: 0169-2070. DOI: 10.1016/j.ijforecast.2021.11.001.
- [14] R. J. Hyndman and G. Athanasopoulos, *Forecasting: principles and practice*, Third. Melbourne, Australia: OTexts, 2021.
- [15] E. Camporeale, X. Chu, O. V. Agapitov, and J. Bortnik, “On the generation of probabilistic forecasts from deterministic models,” *Space Weather*, vol. 17, no. 3, pp. 455–475, 2019. DOI: 10.1029/2018SW002026.
- [16] W. H. Williams and M. L. Goodman, “A simple method for the construction of empirical confidence limits for economic forecasts,” *Journal of the American Statistical Association*, vol. 66, no. 336, pp. 752–754, 1971. DOI: 10.1080/01621459.1971.10482340.
- [17] K. Stankeviciute, A. M. Alaa, and M. van der Schaar, “Conformal time series forecasting,” in *Advances in Neural Information Processing Systems*, M. Ranzato, A. Beygelzimer, Y. Dauphin, P. Liang, and J. W. Vaughan, Eds., vol. 34, Curran Associates, Inc., 2021, pp. 6216–6228.
- [18] Y. Wang, G. Hug, Z. Liu, and N. Zhang, “Modeling load forecast uncertainty using generative adversarial networks,” *Electric Power Systems Research*, vol. 189, p. 106 732, 2020, ISSN: 0378-7796. DOI: 10.1016/j.epsr.2020.106732.
- [19] K. Phipps, B. Heidrich, M. Turowski, M. Wittig, R. Mikut, and V. Hagenmeyer, “Generating probabilistic forecasts from arbitrary point forecasts using a conditional invertible neural network,” *Applied Intelligence*, 2024, ISSN: 1573-7497. DOI: 10.1007/s10489-024-05346-9.
- [20] F. Hutter, L. Kotthoff, and J. Vanschoren, *Automated machine learning: Methods, systems, challenges* (The Springer Series on Challenges in Machine Learning). Cham, Switzerland: Springer International Publishing, 2019. DOI: 10.1007/978-3-030-05318-5.
- [21] M. Rätz, A. P. Javadi, M. Baranski, K. Finkbeiner, and D. Müller, “Automated data-driven modeling of building energy systems via machine learning algorithms,” *Energy and Buildings*, vol. 202, p. 109 384, 2019. DOI: 10.1016/j.enbuild.2019.109384.
- [22] S. Y. Shah *et al.*, “AutoAI-TS: AutoAI for time series forecasting,” in *Proceedings of the 2021 International Conference on Management of Data*, ser. SIGMOD ’21, Virtual Event, China: Association for Computing Machinery, 2021, pp. 2584–2596, ISBN: 9781450383431. DOI: 10.1145/3448016.3457557.
- [23] D. Deng, F. Karl, F. Hutter, B. Bischl, and M. Lindauer, “Efficient automated deep learning for time series forecasting,” in *Machine Learning and Knowledge Discovery in Databases*, M.-R. Amini, S. Canu, A. Fischer, T. Güns, P. Kralj Novak, and G. Tsoumakas, Eds., Cham, Switzerland: Springer Nature, 2023, pp. 664–680, ISBN: 978-3-031-26409-2.

- [24] O. Shchur *et al.*, “AutoGluon–TimeSeries: AutoML for probabilistic time series forecasting,” in *International Conference on Automated Machine Learning*, PMLR, 2023, pp. 9–1.
- [25] C. Debus, M. Piraud, A. Streit, F. Theis, and M. Götz, “Reporting electricity consumption is essential for sustainable AI,” *Nature Machine Intelligence*, vol. 5, no. 11, pp. 1176–1178, 2023, ISSN: 2522-5839. DOI: 10.1038/s42256-023-00750-1.
- [26] D. Salinas, V. Flunkert, J. Gasthaus, and T. Januschowski, “DeepAR: Probabilistic forecasting with autoregressive recurrent networks,” *International Journal of Forecasting*, vol. 36, no. 3, pp. 1181–1191, 2020, ISSN: 0169-2070. DOI: 10.1016/j.ijforecast.2019.07.001.
- [27] S. S. Rangapuram, L. D. Werner, K. Benidis, P. Mercado, J. Gasthaus, and T. Januschowski, “End-to-end learning of coherent probabilistic forecasts for hierarchical time series,” in *Proceedings of the 38th International Conference on Machine Learning*, M. Meila and T. Zhang, Eds., ser. Proceedings of Machine Learning Research, vol. 139, PMLR, 2021, pp. 8832–8843.
- [28] B. Heidrich *et al.*, “Controlling non-stationarity and periodicities in time series generation using conditional invertible neural networks,” *Applied Intelligence*, vol. 53, no. 8, pp. 8826–8843, 2023, ISSN: 1573-7497. DOI: 10.1007/s10489-022-03742-7.
- [29] A. J. Cannon, “Quantile regression neural networks: Implementation in R and application to precipitation downscaling,” *Computers & Geosciences*, vol. 37, no. 9, pp. 1277–1284, 2011, ISSN: 0098-3004. DOI: 10.1016/j.cageo.2010.07.005.
- [30] J. Á. González Ordiano, L. Gröll, R. Mikut, and V. Hagenmeyer, “Probabilistic energy forecasting using the nearest neighbors quantile filter and quantile regression,” *International Journal of Forecasting*, vol. 36, no. 2, pp. 310–323, 2020, ISSN: 0169-2070. DOI: 10.1016/j.ijforecast.2019.06.003.
- [31] R. Wen and T. Kari, “Deep generative quantile-copula models for probabilistic forecasting,” in *Proceedings of the 36th International Conference on Machine Learning*, Paper: Time Series Workshop at ICML 2019, 2019.
- [32] K. Rasul, A.-S. Sheikh, I. Schuster, U. M. Bergmann, and R. Vollgraf, “Multivariate probabilistic time series forecasting via conditioned normalizing flows,” in *International Conference on Learning Representations*, 2021.
- [33] A. Jamgochian, D. Wu, K. Menda, S. Jung, and M. J. Kochenderfer, *Conditional approximate normalizing flows for joint multi-step probabilistic forecasting with application to electricity demand*, 2022. arXiv: 2201.02753.
- [34] M. Arpogaus, M. Voss, B. Sick, M. Nigge-Uricher, and O. Dürr, “Short-term density forecasting of low-voltage load using Bernstein-polynomial normalizing flows,” *IEEE Transactions on Smart Grid*, vol. 14, no. 6, pp. 4902–4911, 2023. DOI: 10.1109/TSG.2023.3254890.
- [35] A. Fanfarillo, B. Roozitalab, W. Hu, and G. Cervone, “Probabilistic forecasting using deep generative models,” *GeoInformatica*, vol. 25, no. 1, pp. 127–147, 2021, ISSN: 1573-7624. DOI: 10.1007/s10707-020-00425-8.
- [36] L. Zhang and B. Zhang, “Scenario forecasting of residential load profiles,” *IEEE Journal on Selected Areas in Communications*, vol. 38, no. 1, pp. 84–95, 2020. DOI: 10.1109/JSAC.2019.2951973.
- [37] L. Ge, W. Liao, S. Wang, B. Bak-Jensen, and J. R. Pillai, “Modeling daily load profiles of distribution network for scenario generation using flow-based generative network,” *IEEE Access*, vol. 8, pp. 77 587–77 597, 2020. DOI: 10.1109/ACCESS.2020.2989350.
- [38] J. Dumas, A. Wehenkel, D. Lanaspèze, B. Cornélusse, and A. Sutera, “A deep generative model for probabilistic energy forecasting in power systems: Normalizing flows,” *Applied Energy*, vol. 305, p. 117 871, 2022, ISSN: 0306-2619. DOI: 10.1016/j.apenergy.2021.117871.
- [39] E. Cramer, D. Witthaut, A. Mitsos, and M. Dahmen, “Multivariate probabilistic forecasting of intraday electricity prices using normalizing flows,” *Applied Energy*, vol. 346, p. 121 370, 2023, ISSN: 0306-2619. DOI: 10.1016/j.apenergy.2023.121370.
- [40] V. Chernozhukov, K. Wüthrich, and Y. Zhu, “Distributional conformal prediction,” *Proceedings of the National Academy of Sciences*, vol. 118, no. 48, e2107794118, 2021. DOI: 10.1073/pnas.2107794118.
- [41] M. Zaffran, O. Féron, Y. Goude, J. Josse, and A. Dieuleveut, “Adaptive conformal predictions for time series,” in *International Conference on Machine Learning*, PMLR, 2022, pp. 25 834–25 866.
- [42] R. J. Hyndman, A. B. Koehler, R. D. Snyder, and S. Grose, “A state space framework for automatic forecasting using exponential smoothing methods,” *International Journal of Forecasting*, vol. 18, no. 3, pp. 439–454, 2002. DOI: 10.1016/S0169-2070(01)00110-8.
- [43] R. J. Hyndman and Y. Khandakar, “Automatic time series forecasting: The forecast package for R,” *Journal of Statistical Software*, vol. 27, no. 3, pp. 1–22, 2008. DOI: 10.18637/jss.v027.i03.
- [44] A. M. De Livera, R. J. Hyndman, and R. D. Snyder, “Forecasting time series with complex seasonal patterns using exponential smoothing,” *Journal of the American Statistical Association*, vol. 106, no. 496, pp. 1513–1527, 2011. DOI: 10.1198/jasa.2011.tm09771.

- [45] S. Maldonado, A. González, and S. Crone, “Automatic time series analysis for electric load forecasting via support vector regression,” *Applied Soft Computing*, vol. 83, p. 105616, 2019. DOI: 10.1016/j.asoc.2019.105616.
- [46] J. M. Valente and S. Maldonado, “SVR-FFS: A novel forward feature selection approach for high-frequency time series forecasting using support vector regression,” *Expert Systems with Applications*, vol. 160, p. 113729, 2020. DOI: 10.1016/j.eswa.2020.113729.
- [47] S. Fan, X. Qin, Z. Jia, X. Qi, and M. Lin, “ELM-based improved layered ensemble architecture for time series forecasting,” *IEEE Access*, vol. 7, pp. 97827–97837, 2019. DOI: 10.1109/ACCESS.2019.2927047.
- [48] F. S. Barros, V. Cerqueira, and C. Soares, “Empirical study on the impact of different sets of parameters of gradient boosting algorithms for time-series forecasting with LightGBM,” in *PRICAI 2021: Trends in Artificial Intelligence*, D. N. Pham, T. Theeramunkong, G. Governatori, and F. Liu, Eds., Cham, Switzerland: Springer International Publishing, 2021, pp. 454–465, ISBN: 978-3-030-89188-6.
- [49] X. Wu, D. Zhang, C. Guo, C. He, B. Yang, and C. S. Jensen, “AutoCTS: Automated correlated time series forecasting,” *Proc. VLDB Endow.*, vol. 15, no. 4, pp. 971–983, 2021, ISSN: 2150-8097. DOI: 10.14778/3503585.3503604.
- [50] W. Kong *et al.*, “Effect of automatic hyperparameter tuning for residential load forecasting via deep learning,” in *2017 Australasian Universities Power Engineering Conference (AUPEC)*, 2017, pp. 1–6. DOI: 10.1109/AUPEC.2017.8282478.
- [51] A. Al Mamun, M. Hoq, E. Hossain, and R. Bayindir, “A hybrid deep learning model with evolutionary algorithm for short-term load forecasting,” in *2019 8th International Conference on Renewable Energy Research and Applications (ICRERA)*, 2019, pp. 886–891. DOI: 10.1109/ICRERA47325.2019.8996550.
- [52] R. C. Smith, *Uncertainty quantification: Theory, implementation, and applications*, First. Philadelphia, USA: Society for Industrial and Applied Mathematics, 2013. DOI: 10.1137/1.9781611973228.
- [53] S. Meisenbacher *et al.*, “Review of automated time series forecasting pipelines,” *WIREs Data Mining and Knowledge Discovery*, vol. 12, no. 6, e1475, 2022. DOI: 10.1002/widm.1475.
- [54] J. Bergstra and Y. Bengio, “Random search for hyperparameter optimization,” *Journal of Machine Learning Research*, vol. 13, pp. 281–305, 2012.
- [55] L. Ardizzone, C. Lüth, J. Kruse, C. Rother, and U. Köthe, *Guided image generation with conditional invertible neural networks*, 2019. arXiv: 1907.02392.
- [56] B. Heidrich, M. Turowski, N. Ludwig, R. Mikut, and V. Hagenmeyer, “Forecasting energy time series with profile neural networks,” in *Proceedings of the Eleventh ACM International Conference on Future Energy Systems*, ser. e-Energy ’20, Virtual Event, Australia: Association for Computing Machinery, 2020, pp. 220–230, ISBN: 9781450380096. DOI: 10.1145/3396851.3397683.
- [57] E. Giacomazzi, F. Haag, and K. Hopf, “Short-term electricity load forecasting using the Temporal Fusion Transformer: Effect of grid hierarchies and data sources,” in *Proceedings of the 14th ACM International Conference on Future Energy Systems*, ser. e-Energy ’23, Orlando, USA: Association for Computing Machinery, 2023, pp. 353–360, ISBN: 9798400700323. DOI: 10.1145/3575813.3597345.
- [58] L. Richter, F. Bauer, S. Klaiber, and P. Bretschneider, “Day-ahead electricity load prediction based on calendar features and temporal convolutional networks,” in *Theory and Applications of Time Series Analysis and Forecasting*, O. Valenzuela, F. Rojas, L. J. Herrera, H. Pomares, and I. Rojas, Eds., Cham, Switzerland: Springer International Publishing, 2023, pp. 243–253, ISBN: 978-3-031-14197-3.
- [59] K. Phipps, S. Meisenbacher, B. Heidrich, M. Turowski, R. Mikut, and V. Hagenmeyer, “Loss-customised probabilistic energy time series forecasts using automated hyperparameter optimisation,” in *Proceedings of the 14th ACM International Conference on Future Energy Systems*, ser. e-Energy ’23, Orlando, USA: Association for Computing Machinery, 2023, pp. 271–286, ISBN: 9798400700323. DOI: 10.1145/3575813.3595204.
- [60] J. Bergstra, D. Yamins, and D. Cox, “Making a science of model search: Hyperparameter optimization in hundreds of dimensions for vision architectures,” in *Proceedings of the 30th International Conference on Machine Learning*, ser. ICML ’13, Proceedings of Machine Learning Research, PMLR, 2013, pp. 115–123.
- [61] O. Taubert *et al.*, “Massively parallel genetic optimization through asynchronous propagation of populations,” in *High Performance Computing*, A. Bhatlele, J. Hammond, M. Baboulin, and C. Kruse, Eds., Cham, Switzerland: Springer Nature, 2023, pp. 106–124, ISBN: 978-3-031-32041-5.
- [62] B. Bischl *et al.*, “Hyperparameter optimization: Foundations, algorithms, best practices, and open challenges,” *WIREs Data Mining and Knowledge Discovery*, vol. 13, no. 2, e1484, 2023. DOI: 10.1002/widm.1484.
- [63] F. Wiese *et al.*, “Open Power System Data: Frictionless data for electricity system modelling,” *Applied Energy*, vol. 236, pp. 401–409, 2019, ISSN: 0306-2619. DOI: 10.1016/j.apenergy.2018.11.097. [Online]. Available: <https://open-power-system-data.org/>.

- [64] A. Trindade, *Electricity load diagrams 2011-2014*, UCI Machine Learning Repository, 2015. DOI: 10.24432/C58C86.
- [65] H. Fanaee-T, *Bike sharing dataset*, UCI Machine Learning Repository, 2013. DOI: 10.24432/C5W894.
- [66] T. Hong, P. Pinson, S. Fan, H. Zareipour, A. Troccoli, and R. J. Hyndman, “Probabilistic energy forecasting: Global energy forecasting competition 2014 and beyond,” *International Journal of Forecasting*, vol. 32, no. 3, pp. 896–913, 2016, ISSN: 0169-2070. DOI: 10.1016/j.ijforecast.2016.02.001.
- [67] T. Gneiting, F. Balabdaoui, and A. E. Raftery, “Probabilistic forecasts, calibration and sharpness,” *Journal of the Royal Statistical Society: Series B (Statistical Methodology)*, vol. 69, no. 2, pp. 243–268, 2007. DOI: 10.1111/j.1467-9868.2007.00587.x.
- [68] J. Beitner. “PyTorch Forecasting.” (2020), [Online]. Available: <https://towardsdatascience.com/introducing-pytorch-forecasting-64de99b9ef46> (visited on 01/02/2021).
- [69] F. Chollet *et al.*, *Keras*, <https://keras.io>, 2015.
- [70] F. Pedregosa *et al.*, “Scikit-learn: Machine learning in Python,” *Journal of Machine Learning Research*, vol. 12, no. 85, pp. 2825–2830, 2011.
- [71] Amazon Web Services, Inc. “Amazon EC2 G4 instances.” (2024), [Online]. Available: <https://aws.amazon.com/ec2/instance-types/g4/> (visited on 05/01/2024).
- [72] C. Ding and H. Peng, “Minimum redundancy feature selection from microarray gene expression data,” in *Computational Systems Bioinformatics. CSB2003. Proceedings of the 2003 IEEE Bioinformatics Conference. CSB2003*, 2003, pp. 523–528. DOI: 10.1109/CSB.2003.1227396.
- [73] D. Werling, M. Beichter, B. Heidrich, K. Phipps, R. Mikut, and V. Hagenmeyer, “The impact of forecast characteristics on the forecast value for the dispatchable feeder,” in *Companion Proceedings of the 14th ACM International Conference on Future Energy Systems*, ser. e-Energy ’23 Companion, Orlando, USA: Association for Computing Machinery, 2023, pp. 59–71, ISBN: 9798400702273. DOI: 10.1145/3599733.3600251.
- [74] M. Löning, A. Bagnall, S. Ganesh, V. Kazakov, J. Lines, and F. J. Király, “sktime: A unified interface for machine learning with time series,” in *2019 Workshop on Systems for ML at NeurIPS*, Vancouver, Canada, 2019.
- [75] Y. Bao, T. Xiong, and Z. Hu, “Multi-step-ahead time series prediction using multiple-output support vector regression,” *Neurocomputing*, vol. 129, pp. 482–493, 2014, ISSN: 0925-2312. DOI: 10.1016/j.neucom.2013.09.010.
- [76] T. Chen and C. Guestrin, “XGBoost: A scalable tree boosting system,” in *Proceedings of the 22nd ACM SIGKDD International Conference on Knowledge Discovery and Data Mining*, ser. KDD ’16, San Francisco, USA: Association for Computing Machinery, 2016, pp. 785–794, ISBN: 9781450342322. DOI: 10.1145/2939672.2939785.

Acronyms

- ANN** Artificial Neural Network
- AR** AutoRegression
- ARIMA** AutoRegressive Integrated Moving Average
- BATS** Box-Cox transformation, ARMA errors, Trend, Seasonal components
- BO** Bayesian Optimization
- CASH** Combined Algorithm Selection and Hyperparameter optimization
- CDF** Cumulative Distribution Function
- cINN** conditional Invertible Neural Network
- CPU** Central Processing Unit
- CRPS** Continuous Ranked Probability Score
- DeepAR** Deep AutoRegression
- DL** Deep Learning
- EA** Evolutionary Algorithm
- ECMWF** European Centre for Medium-Range Weather Forecasts
- ETS** Error Trend Seasonality
- GAN** Generative Adversarial Network
- GBM** Gradient Boosting Machine
- GCP** Grid Connection Point
- GEFCom** Global Energy Forecasting Competition
- GHI** Global Horizontal Irradiance
- GPU** Graphics Processing Unit
- HPC** High-Performance Computing
- HPO** Hyperparameter Optimization
- LASSO** Least Absolute Shrinkage and Selection Operator
- ML** Machine Learning
- MLP** MultiLayer Perceptron
- MRMR** Minimum Redundancy Maximum Relevance
- N-HITS** Neural Hierarchical Interpolation for Time Series
- NNQF** Nearest Neighbor Quantile Filter
- NWP** Numerical Weather Prediction
- OPSD** Open Power System Data
- PDF** Probability Density Function
- PI** Prediction Interval
- PK** Prior Knowledge

PL Pinball Loss

PV PhotoVoltaic

QRNN Quantile Regression Neural Network

RAM Random-Access Memory

RF Random Forest

RNN Recurrent Neural Network

sARIMAX seasonal AutoRegressive Integrated Moving Average with eXternal input

SM Statistical Modeling

SVR Support Vector Regression

TBATS Trigonometric seasonality, Box-Cox transformation, ARMA errors, Trend, Seasonal components

TES Triple Exponential Smoothing

TFT Temporal Fusion Transformer

TPE Tree Parzen Estimator

WP Wind Power

XGB eXtreme Gradient Boosting

Table A3: The CRPS evaluated on the hold-out test subsets before and after post-processing. In post-processing, negative values in the quantile forecasts are set to zero to maintain given limits (mobility indicator, PV generation, and WP generation are greater than or equal to zero). For the other three datasets (Load-BW, Load-GCP, and Price), either no negative values exist in the quantile forecasts, respectively, negative values are valid.

	AutoPQ-default	AutoPQ-advanced	
Mobility	0.2641	0.2585	before post-processing
	± 0.0138	± 0.0051	
PV	0.2627	0.2581	after post-processing
	± 0.0037	± 0.0047	
WP	0.1072	0.1018	before post-processing
	± 0.0003	± 0.001	
WP	0.1060	0.1013	after post-processing
	± 0.0009	± 0.0007	
WP	0.3798	0.3625	before post-processing
	± 0.0018	± 0.0017	
WP	0.3775	0.3621	after post-processing
	± 0.0010	± 0.0012	

Appendix

Table A1: The configuration space Λ_q for the cINN, which transforms a point forecasting model into a probabilistic one, in the respective naming convention [59].

Hyperparameter	Value range	Default value
sampling_std	[0.01, 3.0]	0.1

Table A2: The configuration of the Propulate EA for HPO, in the respective naming convention [61].

Module	Hyperparameter	Value
Islands	generations	-1
	num_isles	2
	migration_probability	0.7
	pollination	True
Compose	pop_size	8
	mate_prob	0.7
	mut_prob	0.4
	random_prob	0.2
	sigma_factor	0.05

Table A4: The configuration spaces Λ_p for the SM-based point forecasting methods in sktime naming convention [74] with the seasonal period $s = 24$.

Forecasting method	Hyperparameter	Value range	Default value
SARIMAX [14]	p	[0, 5]	1
	d	[0, 2]	0
	q	[0, 5]	0
	P	[0, 2]	0
	D	[0, 1]	0
	Q	[0, 2]	0
ExponentialSmoothing [14]	error	{add, mul}	add
	trend	{add, mul, None}	None
	seasonal	{add, mul, None}	None
	damped_trend	{True, False}	False
TBATS [44]	use_trigonometric_seasonality	{True, False}	True
	use_box_cox	{True, False}	False
	use_arma_errors	{True, False}	False
	use_trend	{True, False}	False
	use_damped_trend	{True, False}	False

Table A5: The configuration spaces Λ_p for the ML-based point forecasting methods in the respective naming conventions.

Forecasting method	Hyperparameter	Value range	Default value
MLPRegressor [70]	activation	{logistic, tanh, relu}	relu
	batch_size	{32, 64, 128}	min(200, n_samples)
	hidden_layer_sizes	{([10, 100]), ([10, 100], [10, 100]), ([10, 100], [10, 100], [10, 100])}	(100)
MSVR [75]	C	[0.01, 100]	1.0
	epsilon	[0.001, 1]	0.1
	kernel	{rbf, laplacian, sigmoid}	rbf
XGBRegressor [76]	learning_rate	[0.01, 1]	0.3
	max_depth	[1, 18]	6
	n_estimators	[10, 300]	100
	sub_sample	[0.5, 1.0]	1.0

Table A6: The configuration spaces Λ_p for the DL-based (point) forecasting methods in PyTorch Forecasting naming convention [68].

Forecasting method	Hyperparameter	Value range	Default value
DeepAR [26]	batch_size	{32, 64, 128}	64
	cell_type	{LSTM, GRU}	LSTM
	dropout	[0.0, 0.2]	0.1
	hidden_size	[10, 100]	10
	rnn_layers	[1, 3]	2
NHITS [12]	batch_size	{32, 64, 128}	64
	dropout	[0.0, 0.2]	0.0
	hidden_size	[8, 1024]	512
	n_blocks	{[1], [1, 1], [1, 1, 1]}	[1, 1, 1]
	n_layers	[1, 3]	2
	shared_weights	{True, False}	True
TemporalFusion - Transformer [11]	batch_size	{32, 64, 128}	64
	dropout	[0.0, 0.2]	0.1
	hidden_continuous_size	[8, 64]	8
	hidden_size	[16, 256]	16
	lstm_layers	[1, 3]	1

DeepAR may also provide probabilistic forecasts.

Table A7: Overview of the training, validation, and test sub-sets of the data with hourly resolution used for evaluation, as well as the selected features based on [19]. The names of the target variables and the features refer to the column names in the datasets.

Data set	Target variable	Features	Training sub-set	Validation sub-set	Test sub-set
Load-BW	load_power_statistics	Seasonal features (2), (3), (4) Lag features (1)	[0,4904] (204.3 d)	[4905,7007] (87.6 d)	[7008,8760] (73.0 d)
Load-GCP	MT_158	Seasonal features (2), (3), (4) Lag features (1)	[0,14716] (613.2 d)	[14717,21023] (262.8 d)	[21024,26280] (219.0 d)
Mobility	cnt	Seasonal features (2), (3), (4) Lag features (1) temp hum windspeed weathersit	[0,9824] (409.3 d)	[9825,14034] (175.4 d)	[14035,17544] (146.2 d)
Price	Zonal Price	Seasonal features (2), (3), (4) Lag features (1) Forecast Total Load Forecast Zonal Load	[0,14541] (605.9 d)	[14542,20773] (259.6 d)	[20774,25968] (216.4 d)
PV	POWER	Seasonal features (2), (3), (4) Lag features (1) SSRD TCC	[0,11033] (459.7 d)	[11034,15762] (197.0 d)	[15763,19704] (164.2 d)
WP	TARGETVAR	Seasonal features (2), (3), (4) Lag features (1) U100 V100 Speed100	[0,9400] (391.7 d)	[9401,13430] (167.9 d)	[13431,16789] (139.9 d)

cnt: count; temp: air temperature; hum: humidity; weathersit: weather situation; SSRD: Surface Short-wave (solar) Radiation Downwards; TCC: Total Cloud Cover; U100, V100, Speed100: wind speeds at 100 meters above ground, with the eastward component (U), the northward component (V), and the total wind speed (Speed).

Table A8: The validation CRPS compared for three trial generators in the inner loop of Algorithm 1 (random search, BO-TPE, BO-TPE-PK). Across the six datasets and the nine forecasting methods, only minor differences occur.

	ETS	sARIMAX	TBATS	MLP	SVR	XGB	DeepAR	N-HiTS	TFT	
Load-BW	0.357	0.266	0.259	0.099	0.100	0.079	0.134	0.090	0.107	random search
	± 0.018	± 0.003	± 0.004	± 0.008	± 0.001	± 0.001	± 0.01	± 0.004	± 0.006	BO
	0.357	0.266	0.259	0.103	0.100	0.079	0.133	0.090	0.107	TPE
Load-GCP	0.357	0.277	0.259	0.100	0.101	0.079	0.133	0.089	0.107	BO
	± 0.018	± 0.003	± 0.004	± 0.011	± 0.001	± 0.001	± 0.01	± 0.004	± 0.006	TPE PK
	0.357	0.277	0.259	0.100	0.101	0.079	0.133	0.089	0.107	BO
Load-BW	± 0.018	± 0.014	± 0.004	± 0.008	± 0.001	± 0.001	± 0.01	± 0.002	± 0.006	TPE PK
	0.576	0.491	0.405	0.219	0.215	0.197	0.247	0.230	0.212	random search
	± 0.024	± 0.005	± 0.008	± 0.002	± 0.002	± 0.001	± 0.007	± 0.004	± 0.002	BO
Load-GCP	0.576	0.491	0.405	0.219	0.215	0.197	0.247	0.230	0.212	TPE
	± 0.024	± 0.005	± 0.008	± 0.002	± 0.002	± 0.001	± 0.007	± 0.004	± 0.002	BO
	0.576	0.491	0.405	0.219	0.215	0.197	0.247	0.230	0.212	TPE PK
Mobility	± 0.024	± 0.005	± 0.008	± 0.002	± 0.002	± 0.001	± 0.007	± 0.004	± 0.002	BO
	0.630	0.611	0.446	0.377	0.416	0.397	0.280	0.295	0.261	random search
	± 0.007	± 0.01	± 0.001	± 0.014	± 0.004	± 0.005	± 0.01	± 0.05	± 0.008	BO
Mobility	0.630	0.611	0.446	0.376	0.416	0.397	0.279	0.294	0.261	TPE
	± 0.008	± 0.01	± 0.002	± 0.006	± 0.004	± 0.005	± 0.011	± 0.048	± 0.008	BO
	0.630	0.611	0.445	0.374	0.416	0.397	0.280	0.288	0.261	TPE PK
Price	± 0.007	± 0.01	± 0.002	± 0.006	± 0.005	± 0.005	± 0.01	± 0.036	± 0.007	BO
	0.551	0.252	0.285	0.194	0.205	0.206	0.189	0.164	0.194	random search
	± 0.012	± 0.006	± 0.003	± 0.002	± 0.001	± 0.003	± 0.01	± 0.01	± 0.008	BO
Price	0.550	0.252	0.285	0.196	0.205	0.206	0.190	0.162	0.194	TPE
	± 0.011	± 0.006	± 0.003	± 0.004	± 0.001	± 0.003	± 0.01	± 0.007	± 0.008	BO
	0.550	0.252	0.285	0.194	0.205	0.206	0.191	0.162	0.194	TPE PK
PV	± 0.012	± 0.006	± 0.003	± 0.005	± 0.001	± 0.003	± 0.003	± 0.007	± 0.008	BO
	0.303	0.696	0.165	0.127	0.114	0.107	0.158	0.161	0.131	random search
	± 0.018	± 0.196	± 0.001	± 0.002	± 0.001	± 0.001	± 0.004	± 0.025	± 0.001	BO
PV	0.303	0.695	0.165	0.127	0.114	0.107	0.158	0.168	0.131	TPE
	± 0.018	± 0.196	± 0.001	± 0.002	± 0	± 0.001	± 0.004	± 0.043	± 0.001	BO
	0.303	0.695	0.165	0.127	0.114	0.107	0.158	0.159	0.131	TPE PK
WP	± 0.017	± 0.196	± 0.001	± 0.002	± 0	± 0.001	± 0.005	± 0.023	± 0.001	BO
	0.549	0.497	0.547	0.320	0.303	0.292	0.412	0.389	0.407	random search
	± 0.004	± 0.008	± 0.011	± 0.009	± 0.003	± 0.001	± 0.003	± 0.011	± 0.017	BO
WP	0.549	0.496	0.547	0.321	0.303	0.292	0.412	0.389	0.408	TPE
	± 0.004	± 0.008	± 0.012	± 0.013	± 0.003	± 0.001	± 0.003	± 0.011	± 0.017	BO
	0.549	0.502	0.545	0.319	0.303	0.292	0.412	0.390	0.407	TPE PK
WP	± 0.003	± 0.019	± 0.013	± 0.005	± 0.003	± 0.001	± 0.004	± 0.01	± 0.017	BO